Blocking toxin function and modulating the gut microbiota: caffeic acid phenethyl ester as a potential treatment for *Clostridioides difficile* infection

Yan Guo[1#], Yong Zhang[2#], Guizhen Wang[3], Hongtao Liu[1], Jianfeng Wang[1], Xuming Deng[1], Liuqing He[4*], Jiazhang Qiu[1*]

[1] State Key Laboratory for Diagnosis and Treatment of Severe Zoonotic Infectious Diseases, Key Laboratory for Zoonosis Research of the Ministry of Education, College of Veterinary Medicine, Jilin University, Center for Pathogen Biology and Infectious Diseases, The First Hospital of Jilin University, Changchun, China.

[2] Center for Pathogen Biology and Infectious Diseases, State Key Laboratory for Zoonotic Diseases, The First Hospital of Jilin University, Changchun 130021, China.

[3] Measurement Biotechnique Research Center, College of Biological and Food Engineering, Jilin Engineering Normal University, Changchun 130052, China.

[4] Hunan Provincial Key Laboratory of Animal Intestinal Function and Regulation, Hunan International Joint Laboratory of Animal Intestinal Ecology and Health, Laboratory of Animal Nutrition and Human Health, College of Life Sciences, Hunan Normal University, Changsha, China.

#YG and YZ contributed equally to this work.

*Correspondence: Jiazhang Qiu (qiujz@jlu.edu.cn); Liuqin He (heliuqin@hunnu.edu.cn)

Abstract

Clostridioides difficile infection (CDI) is the leading cause of hospital-acquired diarrhea that seriously threatens public health. The disruption of normal gut microbiota by the use of broad-spectrum antimicrobial agents enables C. difficile to proliferate in the colon. The emergence and prevalence of hypervirulent C. difficile strains result in increased morbidity, mortality, and high recurrence rates of CDI, thus creating a pressing need for novel therapeutics. The multi-domain toxins TcdA and TcdB are the primary determinants of CDI pathogenesis, rendering them ideal drug targets in the anti-virulence paradigm. In this study, we identified caffeic acid and its derivatives from natural compounds library as active inhibitors of TcdB via a cell-based high-throughput phenotypic screening. Further mechanistic investigations revealed that caffeic acid phenethyl ester (CAPE) could directly bind to TcdB, thus suppressing $InsP_6$-induced autoproteolysis and inhibiting glucosyltransferase activity. CAPE treatment remarkably reduces the pathology of CDI in a murine infection model in terms of alleviated diarrhea symptoms, decreased bacterial colonization, and relieved histopathological lesions. Moreover, CAPE treatment of *C. difficile*-challenged mice induces a remarkable increase in the diversity and composition of the gut microbiota (e.g., *Bacteroides* spp.) and alterations of gut metabolites (e.g., adenosine, D-proline, and melatonin), which might partially contribute to the therapeutic outcomes of CAPE against CDI. Our results reveal the potential of CAPE as a therapeutic

for the management of CDI, or CAPE might serve as a lead compound for the development of antivirulence drugs targeting TcdB.

Keywords: *Clostridioides difficile*; toxin B; caffeic acid phenethyl ester; gut microbiota; gut metabolites

Introduction

Clostridioides difficile (*C. difficile*) is an obligate anaerobic, spore-forming, gram-positive bacterial pathogen that is the most common cause of hospital-acquired and antibiotic-associated gastrointestinal diseases, including mild diarrhea and life-threatening pseudomembranous colitis [1, 2, 3]. In the United States, *C. difficile* is responsible for almost half a million infections and approximately 29,000 deaths per year, resulting in an estimated annual healthcare-associated cost of up to $4.8 billion [4, 5]. Importantly, the incidence, severity, mortality and healthcare costs of *C. difficile* infection (CDI) have dramatically increased in the 21st century, at least partially owing to the frequent use of antimicrobial agents and the emergence of hypervirulent strains (e.g., PCR ribotypes 027 and 078) [6, 7, 8]. Limited options are available for the treatment of CDI, while antibiotics including metronidazole, fidaxomicin and vancomycin, are the mainstays of clinical practice [9, 10]. However, antibiotic treatment is ineffective in more than 35% of CDI patients and can lead infection recurrence [11, 12]. Moreover, the rapid evolution of antibiotic resistance in *C. difficile* has further compromised the therapeutic efficacy of current treatment options [13]. Therefore, the high morbidity and mortality, high recurrence rates, and emergence of multiple antibiotic-resistant isolates have made this pathogen a major threat to public health; these factors highlight the urgent need for novel therapies.

C. difficile widely exists in the environment and in the intestinal tract of

humans and animals and is mainly transmitted via the fecal-oral route [14]. The pathogenesis of CDI is correlated with the use of antibiotics, which impair the structure and composition of the normal gut microbiota, thus allowing *C. difficile* to proliferate in the colon [14]. Therefore, previous antibiotic therapy is the major risk factor for the development of CDI. In the colon, the dormant spores of *C. difficile* germinate into oxygen-sensitive vegetative cells that produce toxins and cause symptoms of disease [15]. *C. difficile* secretes two large clostridial exotoxins (TcdA and TcdB), which are directly responsible for the clinical pathology of CDI [16, 17]. Epidemiological studies suggest that most disease-causing *C. difficile* strains have genes that encode TcdB [18, 19]. TcdA and TcdB have identical functional domains: a N-terminal glucosyltransferase catalytic domain (GTD), a cysteine protease active domain (CPD), a transmembrane domain (DRBD), and a C-terminal receptor binding domain (CROPs) [20]. When secreted into the colon, both toxins are internalized by host cells through receptor-mediated, clathrin-dependent endocytosis. Following a decrease in endosomal pH, the toxins undergo conformational changes in the DRBD, resulting in insertion of the toxin into the endosome membrane, pore formation, and the release of the GTD and CPD domains into the cytosol. Then, CPD binding with cytosolic inositol hexakisphosphate ($InsP_6$) activates its protease activity, leading to the cleavage and release of the GTD. Eventually, the GTD utilizes UDP-glucose to glucosylate Rho and/or Ras family GTPases, thus disrupting GTPase signaling and resulting in deleterious effects, including

cytopathic “rounding”, dysregulation of the actin cytoskeleton, apoptosis, and pyroptosis [1]. Although both toxins are cytotoxic to host cells, TcdB shows greater toxicity than TcdA [21].

Disruption of the gut microbiota by antimicrobial agents results in high recurrence rates, which limits the application of antimicrobial therapy for CDI [14]. Consequently, there is a critical need to develop nonantibiotic treatments for CDI, either as standalone or augmented therapies. Importantly, strategies targeting bacterial virulence factors, including toxins, are termed anti-virulence strategies and have attracted interest in the 21st century [22]. Owing to its essential role in *C. difficile* pathogenesis, TcdB has become an ideal target for the development of anti-virulence drugs [23]. In this study, caffeic acid and a series of its derivatives were found to inhibit TcdB-mediated cell rounding via cell-based screening. Among these potential inhibitors, caffeic acid phenethyl ester (CAPE) had the greatest inhibitory effect. Mechanistically, CAPE bound to both full-length TcdB and the GTD fragment, leading to alterations in the secondary structure. This interaction suppressed the $InsP_6$-mediated self-cleavage of TcdB, as well as the enzymatic activity of GTD, thereby decreasing the level of glucosylated Rac1 in TcdB-treated host cells and further inhibiting the cytopathology and cytotoxicity of TcdB. Oral administration of CAPE significantly protected against CDI in models of animal infection. In addition to direct toxin inhibition, the therapeutic effect may also be attributed to CAPE-induced alteration of the gut microbiota (e.g., *Bacteroides*

spp.) as well as gut metabolites (e.g., adenosine, D-proline, and melatonin). Overall, our study revealed that caffeic acid and its derivatives, particularly CAPE, may serve as promising lead compounds for the development of anti-virulence drugs to treat CDI.

Results

CAPE inhibits cell rounding induced by TcdB

TcdB can inactivate Rho GTPases via glucosylation, leading to the loss of cytoskeletal structure and cell-rounding. Consequently, we utilized this phenotype to identify potential TcdB inhibitors from 2076 chemicals, including 1515 FDA-approved drugs and 561 natural compounds. The minimal concentration of recombinant His_6-TcdB (0.2 ng/mL) that induced 100% cell rounding within 1 h was used for drug screening. This concentration of TcdB was preincubated with 8 μg/mL of the individual compounds for 1 h, the compounds that were not bound to TcdB were removed and then added to added to Vero cell cultures. At 1 h post-TcdB treatment, cell morphology was visualized under a light microscope (**Figure 1A**). These analyses allowed us to identify 22 candidate compounds with potent inhibitory effects (**Figure 1B**). Interestingly, six out of the 22 compounds were caffeic acid derivatives. The natural compound library contained eight caffeic acid derivatives, of which methyl caffeic acid and ferulic acid displayed no efficacy. Caffeic acid itself only slightly inhibited TcdB-induced cell rounding, with a 50% inhibitory

concentration (IC_{50}) of 527.5 μg/mL (1.86 mM) (**Table S1**). Notably, except for rosmarinic acid, the IC_{50} values for the other screened caffeic acid derivatives were less than 6 μg/mL, suggesting that these compounds potently inhibited TcdB-mediated toxicity (**Table S1**). CAPE is the phenethyl alcohol ester of caffeic acid and a main active component of propolis with broad pharmacological properties, such as anticancer, anti-inflammatory, antiviral, antibacterial, antifungal, antioxidant, and immunomodulatory activities [24]. As CAPE has the lowest IC_{50} (3.0 μg/mL) among the active caffeic acid derivatives, it was selected as the representative compound for subsequent investigations (**Table S1**). After preincubation with increasing concentrations of CAPE, dose-dependent inhibition of cell rounding was observed in both Vero and HeLa cells (**Figure 1C**). The protective influence of CAPE against TcdB-induced Vero cell death remained evident even when the treatment duration was prolonged to 12 h (**Figure S1A-B**).

In addition, we also determined whether inhibition of TcdB by CAPE could lead to loss of toxin function *in vivo* using a murine systemic intoxication model. A lethal dose of recombinant His_6-TcdB (30 ng) was preincubated with either DMSO or CAPE (2 or 4 μg/mL) for 1 h at 37 ^{o}C, followed by intraperitoneal injection into mice. Notably, all mice in the DMSO group (n=10) died within 36 h after toxin injection. However, 100% of mice pretreated with CAPE 4 (μg/mL) toxin survived at the monitoring endpoint (72 h) (n=10) (**Figure 1D**). Furthermore, we evaluated the efficacy of CAPE following an intraperitoneal

injection by administering it 2 h prior to the injection of TcdB, in order to gauge the survival rate of the mice. The outcomes revealed that a 2 h pretreatment with CAPE at doses of 30 and 50 mg/kg significantly enhanced the mice's protection rate by 57.1% (**Figure S2)**. Simultaneously, we assessed the impact of CAPE on *C.difficile* itself. CAPE markedly repressed *tcdB* gene expression at a concentration of 16 μg/mL (**Figure S3A**) and inhibited the growth and spore formation of *C. difficile* BAA-1870 at a concentration of 32 μg/mL (**Figure S3B-C**). Taken together, these data indicate that CAPE is a potent toxin inhibitor of TcdB and may serve as a promising antimicrobial agent.

CAPE decreases $InsP_6$-induced autoproteolysis of TcdB and inhibits the enzymatic activity of GTD

TcdB is a multi-domain containing toxin that induces toxicity in host cells via an intricate and multistep mechanism. This mechanism involves (i) receptor-mediated endocytosis, (ii) pore formation and subsequent membrane translocation, (iii) autoproteolysis and release of GTD, and (iv) the glucosylation of small GTPases (**Figure 2A**). To determine the mechanism by which CAPE suppresses the cytotoxicity of TcdB, we first labeled full-length TcdB with Alexa Fluor 488; then, the concentration of the endocytosed toxin was determined via flow cytometry. Apparently, incubation of CAPE with TcdB did not significantly affect its entry into host cells (**Figure 2B**). Next, we stained CAPE-treated cells with LysoTracker, a fluorescent dye that accumulates in

186 the acidic organelles of live cells. In contrast to the vacuolar-type H+-ATPase
187 (V-ATPase) inhibitor bafilomycin A1 (Baf-A1), CAPE treatment did not alter the
188 intensity of LysoTracker fluorescence staining in either THP-1 or Caco-2 cells,
189 suggesting that inactivation of TcdB by CAPE is not due to changes in the pH
190 of endosomal compartments (**Figure 2C-D** and **Figure S4A-B**).

191 These observations indicate that CAPE might exert its effects after
192 membrane translocation. Indeed, preincubation of full-length TcdB with CAPE
193 blocked the $InsP_6$-induced autoproteolysis of TcdB, as revealed by the gradual
194 decrease in the production of released GTP, followed by the addition of
195 increasing amounts of CAPE *in vitro* (**Figure 2E-F**). Furthermore, we
196 determined the glucosyltransferase activity using recombinant GTD in the
197 absence or presence of different doses of CAPE. Strikingly, incubation with 2
198 μg/mL CAPE resulted in a significant reduction in GTD activity, whereas 32
199 μg/mL CAPE compromised 87.5% of the enzymatic activity (**Figure 2G**).
200 Importantly, in response to suppression of $InsP_6$-induced autoproteolysis and
201 GTD function, treatment of TcdB-challenged cells with CAPE markedly
202 decreased the level of glucosylated Rac1 in a dose-dependent manner
203 (**Figure 2H-I**). Taken together, these results suggest that CAPE disrupts
204 $InsP_6$-induced autoproteolysis of TcdB and inhibits the enzymatic activity of
205 GTD, thereby decreasing the glucosylation of Rac1 and alleviating cell
206 rounding.

207 **CAPE alters the secondary structure of full-length TcdB and GTD**

To further clarify the mechanisms used by CAPE to inactivate TcdB, we determined the secondary structures of full-length TcdB and GTD in the absence or presence of CAPE by circular dichroism spectroscopy. Apparently, incubation of CAPE with full-length TcdB resulted in a significant increase in the α-helix content (15.4% to 21.0%) and a concomitant decrease in the β-pleated sheet content (34.5% to 20.9%) (**Figure 3A-B**). Similarly, the secondary structure of GTD was markedly altered upon incubation with CAPE, with the proportion of α-helices decreasing from 37.9% to 0.0% and the proportion of β-pleated sheets decreasing from 37.2% to 10.9% (**Figure 3C-D**). Taken together, these data suggest that CAPE may interact with full-length TcdB and GTD to induce conformational changes, thus impairing their functions.

CAPE directly interacts with full-length TcdB and GTD

To investigate the potential interaction between CAPE and TcdB or GTD, the binding constants were determined by surface plasmon resonance (SPR) analysis. The results showed that CAPE has strong binding affinity with full-length TcdB and GTD, and the KD values were 1.269×10^{-5} M and 1.007×10^{-3} M, respectively (**Figure 4A-B**). The interaction between CAPE and TcdB exhibits a slow approach to equilibrium, which may primarily be attributed to the rapid occupation of the protein's primary binding sites by the small molecule during the initial phase. Following this, CAPE proceeds to bind to sites with secondary or reduced affinity, a process that prolongs the time

required to achieve equilibrium. Furthermore, the possibility that CAPE binds to multiple sites on TcdB necessitates a duration for the exploration and occupation of these various sites before equilibrium is established. These data demonstrate the direct interaction between CAPE and full-length TcdB/GTD.

Next, we performed molecular docking and molecular simulation dynamics analyses to investigate the interaction between CAPE and GTD (**Figure 5A**). The results revealed that Leu265, Asp286, Thr465, Ile466, Leu519, and Trp520 in GTD were potential binding sites for CAPE (**Figure 5A**). The root mean square deviation (RMSD) of the GTD/CAPE complex was stable over a 100 ns period of simulation (**Figure 5B**). Further energy decomposition analysis showed that the side chains of Leu265, Thr465, Leu519, and Trp520 of GTD contributed to binding with CAPE via van der Waals interactions, among which Trp520 had the highest binding energy (**Figure 5C**). Moreover, we mutated each of the residues that were involved in binding and subsequently determined their glucosyltransferase activities in the presence or absence of CAPE. The enzymatic activities of these mutants were similar to that of wild-type GTD (**Figure 5D**). Mutations in GTD_{L265A}, GTD_{T465A}, GTD_{I466A}, and GTD_{L519A} did not affect the inhibitory effect of CAPE (**Figure 5E-I**). However, the inhibition of GTD_{W520A} and GTD_{D286A} by CAPE was notably compromised (**Figure 5J-K**).

CAPE treatment reduces the pathology of CDI in a murine model

The abovementioned observation that CAPE suppresses the function of

TcdB prompted us to further evaluate the potential therapeutic effects of this compound in CDI. To this end, we employed a well-established murine model in which infected mice can develop symptoms resembling those observed in human CDIs (25). First, cytotoxicity measurements revealed that the viability of both THP-1 and Vero cells was not affected by CAPE treatment (**Figure S5A-B**), thus indicating low toxicity. Mice were preconditioned with drinking water containing 0.5 g/L cefoperazone for 5 days, followed by normal drinking water for 2 days. After challenge with *C. difficile* BAA-1870 via gavage, mice were then treated daily with either vehicle or 30 mg/kg CAPE by gavage throughout the disease course (day 0 to day 5) (**Figure 6A**). Severe weight loss in *C. difficile*-infected mice was observed on days 2 and 3 post infection and was accompanied by diarrhea (**Figure 6B**). Notably, compared to the infection control group, CAPE treatment significantly increased the dry/wet weight ratio of the mouse feces, suggesting the alleviation of diarrhea symptoms (**Figure 6C**). Correspondingly, the weight loss of mice was relieved upon receiving CAPE (**Figure 6B**). Moreover, fecal pellets collected on day 3 were used to determine the bacterial burden. The results revealed that CAPE treatment significantly decreased the number of *C. difficile* CFUs (**Figure 6D**). On day 3 post-*C. difficile* infection, the colon was collected for histopathological analysis. Remarkably, *C. difficile*-infected mice exhibited conspicuous colon edema, epithelial cell injury and inflammatory factor infiltration (**Figure 6E**). In contrast, these histopathological lesions were

significantly less common in mice administered CAPE (**Figure 6F**). Taken together, these data demonstrate the efficacy of CAPE in the treatment of CDI.

CAPE induces distinct microbiota changes in CAPE-treated mice when compared with model mice

Antibiotic-induced dysbiosis of the gut microbiota promotes the development of CDI [25]. Therefore, we next determined whether CAPE has any impact on gut microbial communities that may contribute to its therapeutic efficacy. To this end, on the 3rd day after *C. difficile* challenge, fecal samples from the model group and CAPE treatment group were collected and subjected to microbiota analysis via 16S rRNA gene sequencing. Remarkably, as reflected by the Venn diagram, CAPE treatment resulted in significant changes in the microbial composition compared to those in the model group, and only 16.42% of the operational taxonomic units (OTUs) were shared (**Figure 7A**). In addition, both the α- and β-diversity of the gut microbiota in CAPE-treated mice were significantly greater than those in model mice. Specifically, the increase in the Chao1 richness estimator of mice in the CAPE treatment group suggested a greater number of microbial species and increased evenness in the fecal samples (**Figure 7B-C**); the increase in the Shannon□Wiener diversity index and the Simpson diversity index reflected a significant increase in microbiota diversity (**Figure 7D-E**). Principal coordinate analysis (PCoA) revealed distinct confidence ellipses between the bacterial

communities of the CAPE-treated group and the model group, thereby revealing substantial differences in their microbiota profiles (**Figure 7F**).

A comparative analysis was performed to examine changes at the phylum level following CAPE treatment. *Bacteroidota*, *Firmicutes,* and *Proteobacteria* were the major constituents in both the CAPE treatment and model groups, suggesting that the administration of CAPE did not significantly alter the mouse microbiota at the phylum level (**Figure 7G**). Next, we compared the 10 most abundant TAXA at the genus level. Notably, CAPE treatment markedly elevated the abundance of *Bacteroides* and decreased the abundance of *Muribaculaceae* and *Parabacteroides* (**Figure 7H**). Leveraging linear discriminant analysis of effect sizes (LEfSe), the microbiota was examined at the genus level to identify bacteria exhibiting substantial differences in abundance between the two cohorts (LDA score > 3.5, $p < 0.05$). After CAPE treatment, the relative abundance of *Bacteroides*, *Ruminococcus_gnavus_group*, *Muribaculum* and *Faecalibaculum* OTUs notably increased, while that of *Hungatella*, *Parasutterella* and *Muribaculaceae* OTUs significantly decreased (**Figure 7I**). *Bacteroides*, *Muribaculum* and *Faecalibaculum* improve colonization resistance to *C. difficile* [26, 27, 28]. Importantly, the abundance of these bacterial species increased following CAPE treatment (**Figure 7J-L**). In contrast, the abundance of *Parasutterella*, a bacterium that facilitates *C. difficile* colonization [29], was reduced in mice

316 receiving CAPE (**Figure 7M**). Taken together, these findings suggest that
317 CAPE treatment accelerates microbiota recovery during CDI.

318 **CAPE alters the levels of gut metabolites in *C. difficile*-infected mice**

319 In addition to the crucial role of the gut microbiota in conferring
320 colonization resistance against *C. difficile*, gut microbiota-derived metabolites
321 significantly contribute to the disease process [30]. Metabolomic analysis was
322 performed to evaluate the effects of CAPE treatment on gut metabolites in
323 mice. On the 3rd day after infection, the feces of mice in each group were
324 frozen by liquid nitrogen for metabolomics analysis. The PLS-DA model
325 exhibited significant separation of clusters between the model and CAPE
326 treatment groups (**Figure 8A**). Among the 1599 metabolites, 109 showed
327 substantial differences in levels between the two groups. Specifically,
328 CAPE-treated mice exhibited 19 metabolites with upregulated expression and
329 50 metabolites with downregulated expression compared to those in the model
330 group (fold change > 1.5, $p < 0.05$) (**Figure 8B**). Furthermore, KEGG
331 enrichment analysis revealed that the differentially abundant metabolites were
332 significantly enriched in the purine metabolism and bile secretion pathways
333 (**Figure 8C**). Adenosine is an endogenous purine nucleoside that binds to
334 specific cell surface receptors to exert anti-inflammatory effects at high
335 concentrations [31]. Importantly, CAPE treatment of *C. difficile*-infected mice can
336 increase the adenosine concentration in the gut (**Figure 8D**), which might be
337 attributed to its inhibition of xanthine oxidase [32]. Similarly, the levels of uric acid,

the final product of purine metabolism, were markedly degraded in mice after receiving CAPE (**Figure 8D**). An earlier study reported that increasing the gut adenosine concentration with an adenosine deaminase inhibitor prevents *C. difficile* toxin A-induced enteritis in mice [33]. Therefore, the increase in gut adenosine induced by CAPE might play an important role in its therapeutic efficacy in CDI.

C. difficile predominantly utilizes sugars and amino acids for energy production through various metabolic pathways, such as fermentation [34]. Notably, Stickland fermentation, a Clostridia-specific type of amino acid fermentation, is associated with *C. difficile* pathogenesis [34]. D-proline is one of the preferred nutrients used by *C. difficile* in the Stickland reaction and is critical for its growth [35, 36]. Interestingly, treatment of *C. difficile*-infected mice with CAPE significantly reduced gut D-proline levels (**Figure 8D**). In addition, the metabolomics data also revealed a dramatic increase in the level of melatonin (**Figure 8D**), which is a ubiquitous indolamine that was previously shown to decrease the rate of recurrent CDI [37]. Consistently, quantification of the melatonin content in mouse fecal supernatants using a melatonin detection kit revealed elevated levels of melatonin in CAPE-treated mice (**Figure S6**). Moreover, correlation analysis revealed a positive association between *Faecalibaculum* abundance and melatonin levels (**Figure S7**). Taken together, these results indicate that alterations in gut metabolites caused by CAPE treatment might contribute to its therapeutic efficacy in CDI.

Oral administration of melatonin alleviates the symptoms of CDI

Next, we investigated whether any of the upregulated metabolites had a direct influence on TcdB. To this end, we preincubated recombinant TcdB with each of the selected metabolites prior to addition to the cell cultures. Interestingly, treatment with TcdB and 100 μg/mL melatonin significantly alleviated the cell death induced by this toxin (**Figure 9A**). This observation prompted us to investigate the direct therapeutic potential of melatonin in CDI. Therefore, *C. difficile*-infected mice were orally administered 200 mg/kg melatonin at 24 h intervals. The weight changes and the dry/wet ratio of the stool samples were monitored daily for three days. The results showed that melatonin-treated mice displayed remarkable alleviation of diarrhea, as manifested by notable improvements in weight recovery and a significant increase in the dry/wet weight ratio on the 2nd and 3rd days after *C. difficile* challenge (**Figure 9B-C**). Consistent with these observations, histopathological assessment of colonic tissue sections also revealed attenuated colon damage upon melatonin treatment (**Figure 9D-E**). Taken together, these data indicate that a high dose of exogenous melatonin could protect mice from CDI and that the CAPE-induced increase in endogenous melatonin might improve the therapeutic outcome of patients with CAPE.

Discussion

C. difficile has become the prevalent agent of nosocomial diarrhea and

substantially threatens public health. In particular, the increase in morbidity and mortality caused by the prevalence of hypervirulent and drug-resistant strains has become a global concern [7]. In 2019, *C. difficile* was listed by the US Centers for Disease Control and Prevention as an “urgent threat” that surpassed methicillin-resistant *Staphylococcus aureus* (MRSA) and ESBL-producing *Enterobacterales* [38]. *C. difficile* is a commensal bacterium that colonizes the lower gastrointestinal tract [39]. CDI typically occurs in susceptible individuals whose normal gut microbiota is disrupted by the administration of broad-spectrum antibiotics [39]. Although CDI is considered an antibiotic-associated disease, the current treatment for CDI still relies on antimicrobial drugs, including metronidazole, fidaxomicin and vancomycin [9, 10]. Despite antibiotic therapy, more than 35% of CDI patients are susceptible to recurrent infection, which is primarily attributable to the intrinsic effects of antimicrobial agents, which disrupt the microbiota [12]. In addition, long-term administration of antibiotics promotes the selection of antibiotic-resistant subpopulations in the gut, thus increasing the risk of infections caused by antibiotic-resistant and opportunistic bacteria [40]. As a result, the development of nonantibiotic therapeutics is needed for the treatment of CDI.

Indeed, numerous novel treatments for CDI are being investigated, among which the anti-virulence strategy represents one of the most promising and successful therapeutic approaches [22, 41]. Unlike antibiotics, which target bacterial components that are critical for bacterial growth, anti-virulence drugs

aim to disarm pathogenic bacteria by neutralizing their virulence factors [42, 43]. Therefore, this strategy imposes less selective pressure that directs bacterial evolution of antimicrobial resistance [43]. The disease progression of CDI is strictly dependent on large clostridial toxins (TcdA and TcdB), as strains lacking both toxins (i.e., A^-B^-) were completely avirulent and failed to induce any discernable disease symptoms in a hamster model of infection [44]. Importantly, epidemic *C. difficile* strains with increased morbidity and mortality rates produce greater amounts of toxins [45]. Based on these premises, TcdA and TcdB are considered ideal drug targets for CDI in the anti-virulence paradigm [46]. Indeed, bezlotoxumab, a fully humanized monoclonal antibody that neutralizes TcdB, was approved by the FDA and used in CDI patients to reduce the rate of recurrence [47]. This achievement has encouraged researchers to develop next-generation anti-virulence treatments. In particular, small molecule inhibitors of toxin production and/or activity have attracted increasing interest owing to their advantages in cost and the convenience of oral administration [41]. The multidomain architecture and mechanisms of action of clostridial toxins have provided distinct options for blocking their toxicity. Indeed, previous efforts have identified diverse inhibitors that act on distinct steps of intoxication, such as the inhibition of toxin binding to cell receptors, the suppression of endosomal maturation, and the inactivation of GTD or CPD activities [23, 48, 49, 50, 51]. Although which approach is the best remains unknown, we believe that an inhibitor that targets multiple steps of intoxication would be

superior to those that act on a single step. In this study, we identified a series of caffeic acid derivatives that were potent inhibitors of TcdB via a phenotypic screen. Further mechanistic study revealed that CAPE, the phenethyl alcohol ester of caffeic acid, could block $InsP_6$-induced autoproteolysis of TcdB and inactivate its GTD function (**Figure 10**). Moreover, CAPE treatment significantly protected against CDI in a mouse model of infection. Our results suggested that caffeic acid derivatives, particularly CAPE, are promising lead compounds for the development of anti-virulence drugs that target TcdB. CAPE is a major component of propolis, a natural bee-produced substance that has been used as a remedy for thousands of years in Europe and Asia [52]. As a result, further investigations on the therapeutic potential of propolis against CDI, either in combination with standard therapy or as a single therapy, would be of great interest.

Antibiotic-induced gut microbiota dysbiosis is a major risk factor for CDI [53]. Thus, reconstituting the gut microbiota is a promising strategy for CDI therapy. Fecal microbiota transplantation (FMT) is considered an effective CDI therapeutic strategy and is widely used in clinical practice [54]. Despite the high cure rate and increasing popularity of FMT, patients remains limited acceptance. Another prominent advantage of anti-virulence drugs is that they allow maintenance of the normal microbiota, which is of critical importance for the treatment of CDI. Importantly, CAPE treatment of *C. difficile*-infected mice restored the structure and composition of the microbiota (**Figure 10**). In

particular, the abundance of *Bacteroides*, a critical gut microbiota component that is required for resistance to *C. difficile* colonization [26, 55, 56, 57], was significantly elevated upon CAPE treatment. Interestingly, *Bacteroides* were also predominant in CDI patients administered RBX2660 (Rebyota), an FDA-approved fecal microbiota product [58, 59]. The increased diversity of the gut microbiota might contribute to the therapeutic effects of CAPE in CDI.

In addition to the microbiota, gut metabolites also play crucial roles in the pathogenesis of CDI, either by promoting or suppressing disease progression [30]. For example, bile acids and amino acids promote spore germination and pathogenesis, while secondary bile acid and short-chain fatty acids aid in colonization resistance and suppress spore germination [30]. In addition to restoration of the gut microbiota, metabolomics analysis of mouse fecal samples revealed dramatic alterations in gut metabolites upon CAPE treatment (**Figure 10**). The differentially abundant metabolites were significantly enriched in the purine metabolism and bile metabolism pathways. Remarkably, the level of adenosine, an endogenous purine nucleoside that can regulate immune responses and inflammatory processes by binding to its receptors, such as its ability to inhibit the release of certain inflammatory mediators, was dramatically increased in CAPE-treated mice [60, 61]. In contrast, the amount of uric acid, the final product of purine metabolism, was reduced. Previous studies showed that the increase in adenosine concentrations caused by the inhibition of adenosine deaminase via EHNA prevents *C. difficile*

470 TcdA-mediated damage and inflammation [33]. This protection might be a result
471 of the anti-inflammatory effects of adenosine, which rely on the activation of its
472 receptors [62]. In addition, we observed a reduction in the amount of D-proline,
473 which is one of the preferred amino acids utilized by *C. difficile* to generate
474 energy through Stickland reactions [35]. Melatonin is a ubiquitous indolamine
475 that has broad biological activities [63]. Notably, we detected a significantly
476 increase in the amount of melatonin in the feces of mice that were
477 administered CAPE. Importantly, an earlier study demonstrated a decreased
478 risk of recurrent CDI in patients exposed to melatonin, possibly owing to its
479 antibacterial and anti-inflammatory activities [37]. In this study, we found that oral
480 administration of exogenous melatonin alleviated the symptoms of CDI in a
481 mouse model of infection. Although determining the exact mechanism will
482 require further investigation, we propose that the melatonin-mediated inhibition
483 of TcdB intoxication observed in this study might contribute to its therapeutic
484 effect. Taken together, these results indicate that the alterations in gut
485 metabolites caused by CAPE might also contribute to treatment outcomes for
486 CDI patients.
487

488 **Methods**

489 **Cell lines**

490 All cell lines (HeLa, Caco-2, Vero, HEK293T and THP-1) were obtained
491 from ATCC (Manassas, VA). HeLa, Caco-2, Vero and HEK293T cells were

492 cultured in Dulbecco's modified Eagle's medium (DMEM) (Invitrogen, Carlsbad,
493 CA) supplemented with 10% fetal bovine serum (FBS) (Invitrogen) and 1%
494 (w/v) penicillin streptomycin. THP-1 cells were cultured in Roswell Park
495 Memorial Institute (RPMI) 1640 medium (Invitrogen) supplemented with 10%
496 FBS and 1% (w/v) penicillin streptomycin. All cell lines were cultured at 37 °C
497 in a 5% CO_2 atmosphere.

498 **Bacterial strains and reagents**

499 *C. difficile* BAA-1870 (RT027/ST1) was kindly provided by Aiwu Wu
500 (Guangzhou Medical University) and cultured in brain-heart infusion broth (BHI)
501 supplemented with 5 g/L yeast extract and 0.1% (w/v) L-cysteine (BHIS). The
502 compounds were identified from two main sources: FDA-approved drugs
503 obtained from ApexBio Technology (Houston, TX, USA) and small molecule
504 natural compounds obtained from Chengdu Ruifensi Biotechnology Co., Ltd.
505 (Chengdu, China). LysoTracker Red DND-99, kanamycin, and cefoperazone
506 sodium were purchased from Dalian Meilun Biotechnology Co., Ltd. (Dalian,
507 China).

508 **Mice**

509 Male C57BL/6 mice aged 6-8 weeks were purchased from Liaoning
510 Changsheng Biotechnology Co., Ltd., and housed in a specific pathogen-free
511 (SPF) facility. The mice lived in a controlled environment with a temperature of
512 23±2 °C and a humidity of 55±10 °C. Prior to infection, the mice were
513 acclimated to the environment for a minimum of one week. All mouse

experiments were approved by the Jilin University Institutional Animal Care Committee, Jilin University and strictly conducted according to the guidelines of this committee (SY202402301).

Protein expression and purification

The expression and purification of full-length TcdB were conducted following the method described by *Yang* et al. [64]. In brief, *Bacillus megaterium* harboring pHis1522-TcdB was inoculated into LB media supplemented with a final concentration of 10 μg/mL tetracycline. Once the $OD600_{nm}$ reached approximately 0.3, xylose (0.5% w/v) was added to induce protein expression at 37 °C for 16 h. Then, 100 mL of the bacterial cells was harvested by centrifugation, resuspended in 5 mL of lysis buffer containing 20 mM imidazole, 300 mM NaCl, 20 mM NaH_2PO_4, 500 μM EDTA, and protease inhibitor cocktail (adjusted to pH 8.0), and subjected to sonication. The cell lysate was then centrifuged at 13,400 × g for 20 min to remove cell debris. The TcdB protein was purified using nickel column affinity chromatography. The purity of the protein was confirmed by SDS□PAGE, and the protein was subsequently dialyzed against buffer containing 10% glycerol, 20 mM Tris (pH 7.5), and 150 mM NaCl. After the protein concentration was determined, the purified TcdB protein was aliquoted and stored at -80 °C for further use.

For the purification of GTD, amplified DNA products were inserted into pET28a (Novagen), and the *Escherichia coli* (*E. coli*) strain BL21 (DE3) was used for the expression and purification of GTD. Transformed *E. coli*

pET28a-GTD was cultured in Luria–Bertani (LB) medium supplemented with 10 μg/mL kanamycin. Once the OD600 reached 0.6, the expression of proteins was induced with 0.2 mM isopropyl-β-d-thiogalactoside (IPTG) overnight at 18 °C. The bacterial cells were then harvested by centrifugation and subjected to sonication. The cell lysate was then centrifuged at 13,400 × g for 20 min to remove cell debris. GTD protein was purified using nickel affinity chromatography and dialyzed in buffer containing 10% glycerol, 20 mM Tris (pH 7.5), and 150 mM NaCl. The GTD mutants were introduced into pET28a-GTD using the Quick Change Site-Directed Mutagenesis Kit (Stratagene, San Diego, CA, USA) with the primers listed in **Table S2.** The subsequent purification was performed using the same procedure as described for wild-type GTD.

Reverse transcription-quantitative PCR

Total RNA was extracted by TRIzol and then reverse-transcribed into complementary DNA by a NovoScript® Plus All-in-one 1st Strand cDNA Synthesis SuperMix (E047; Novoprotein, China). mRNA expression of *tcdB* was measured by quantitative PCR with NovoScript®SYBR qPCR SuperMix Plus (E096; Novoprotein, China) using the primers shown in **Table S3**. 16S rRNA was used as internal control. The relative mRNA expression levels were calculated by the delta-delta CT method.

Growth curve assays

Growth curve assay was performed to estimate the influence of CAPE on

the growth of *C. difficile* BAA-1870. The overnight culture of BAA-1870 was transferred to fresh BHIS medium and incubated at 37°C in an anaerobic atmosphere. The culture was supplemented with different concentrations of CAPE ranging from 0 to 64 μg/mL and the optical density at 600 nm was monitored at 4 h intervals to assess growth of BAA-1870.

Inhibition of spore outgrowth

The impact of CAPE on the sporulation of *C. difficile* BAA-1870 was assessed using the protocol described by Joshua *et al* [65]. In brief, BAA-1870 cultures were treated with 8 or 32 μg/mL of CAPE for 48 h. The treated samples were then harvested, subjected to a double wash with PBS, and incubated in a 60°C water bath for 30 min. Subsequently, 20 μL of each spore suspension was plated onto BHIS agar supplemented with 0.1% taurine to facilitate germination. These plates were incubated anaerobically at 37°C for 5 d to allow for spore germination. Following this period, the number of resulting colonies on the plates was enumerated.

Cell rounding assay

Cell rounding assay was performed according to Kristina *et al*, with appropriate adjustments [48]. Vero or HeLa cells were seeded in 96-well sterile plates using serum-free DMEM overnight, and the compounds were preincubated with TcdB for 1 h. After incubation, the TcdB-compound complex was added to cells for 1 h at 37 °C. The cell morphology was visualized under a light microscope.

580 **LysoTracker assay**

581 The pH of endosomes was determined by LysoTracker Red DND-99 [49].
582 Caco-2 or THP-1 cells in complete DMEM were seeded in 96-well sterile
583 plates overnight. The media was changed to serum-free DMEM for 1 h, and
584 CAPE was preincubated with TcdB for 1 h, followed by addition to the cells and
585 incubation for 2 h. Baf-A1 served as a control. After incubation, LysoTracker
586 and Hoechst dyes were added and the cells were incubated for 1 h. Excess
587 dye was removed by changing the media, and alterations in lysosomal red
588 intensity were documented using a fluorescence microscope.

589 ***In vitro* TcdB autoprocessing assay**

590 The self-cleavage ability of TcdB primarily depends on its cysteine
591 protease activity [48]. CAPE (1-16 μg/mL) was preincubated with TcdB for 1 h,
592 followed by the addition of $InsP_6$ and incubation at 37 °C for 6 h. Subsequently,
593 loading buffer was added for SDS□PAGE analysis, and the results were
594 visualized using Coomassie Brilliant Blue staining.

595 **Rac1 glucosylation assay**

596 Rac1 glucosylation assay was performed following the method described
597 by John *et al* [50]. HEK293T cells were seeded into a 6-well plate. The next day,
598 TcdB and different concentrations of CAPE (4-32 μg/mL) were added to cells.
599 After 2 h, the cells were harvested, lysed using lysis buffer, and subjected to
600 centrifugation at 13,400 × g for 10 min to collect the supernatant. The collected
601 supernatant was then mixed with loading buffer and subjected to SDS□PAGE

602 followed by western blot analysis. The glycosylation level of Rac1 was
603 evaluated by determining the levels of non-glycosylated Rac1 (BD Biosciences,
604 Mississauga, ON) and total Rac1 (Abcam).

605 **UDP-Glo^{TM} UDP-glucose hydrolase assay**

606 GTD activity was assessed according to the manufacturer's instructions [50].
607 A total volume of 16 μL, consisting of 100 nM GTD, various concentrations of
608 CAPE and glucosylation buffer, was prepared. Four microliters of UDP-glucose
609 at a final concentration of 25 μM was added to the mixture, which was then
610 allowed to react at room temperature for 15 min. To stop the reaction, 10 μL of
611 the reaction mixture was removed and placed in a white polystyrene 96-well
612 plate containing 10 μL of UDP detection reagent. The reaction took place at
613 room temperature for 1 h. The luminescence value was measured at a 750 ms
614 integral, and the GTD activity was determined based on these measurements.

615 **Circular dichroism (CD) spectroscopy**

616 CD spectra of TcdB, TcdB-CAPE, GTD, and GTD-CAPE were obtained
617 using a CD spectrophotometer (MOS-500; Bio-Logic, France). TcdB or GTD at
618 a concentration of 0.2 mg/mL was incubated with 32 μg/mL CAPE. Changes in
619 the secondary structure of TcdB or GTD were assessed at room temperature
620 using a quartz cuvette with an optical path length of 1 mm. The scan
621 wavelength range was set from 190 to 250 nm with a resolution of 0.2 nm and
622 a bandwidth of 1 nm. The secondary structures of TcdB, TcdB-CAPE, GTD,
623 and GTD-CAPE were analyzed using the BeStSel web server.

Molecular docking

CAPE was obtained as a ligand from PubChem, and its topology was generated using AmeberTools. The crystal structure of GTD was retrieved from the Protein Data Bank (PDB) and processed using AutoDockTools. Docking calculations were performed using AutodockVina, and molecular dynamics simulations were carried out using Gromacs 2020.6. The RMSD of the receptor and ligand was monitored to assess conformational changes during the binding process. The interaction energy was analyzed using the Poisson-Boltzmann surface area (MM-PBSA) method, which is a molecular mechanics approach.

Flow cytometry

Flow cytometry was used to quantify the cellular uptake of TcdB via endocytosis. To facilitate detection, full-length TcdB was labeled with Alexa Fluor®488 NHS Ester (Yeasen Biotechnology Co., Ltd., Shanghai, China). Prior to cell treatment, Alexa Fluor 488-TcdB was preincubated with CAPE at a concentration of 32 μg/mL for 30 min. The treated solution was then added to Caco-2 cells and incubated for 1 h at 37 °C. Following three washes with phosphate-buffered saline (PBS), the Caco-2 cells were collected, and the fluorescence signal was measured using flow cytometry.

Cytotoxicity assay

Vero or THP-1 cells were plated into 96-well plates. The next day, different concentrations of CAPE were prepared by diluting them in DMEM and adding

them to the cells. After incubation at 37 °C for 3 h, the viability of cells was assessed using a Cell Counting Kit-8 (CCK-8) (Beyotime Biotechnology Co., Shanghai, China) according to the manufacturer's instructions.

Biacore analysis

The affinity analysis of TcdB or GTD with CAPE was conducted using a Biacore T100 device (Biacore Inc., Uppsala, Sweden) according to the manufacturer's protocol. A CM5 chip (General Electric Company, GE) was utilized to immobilize the TcdB or GTD proteins. Various concentrations of CAPE were injected, and all steps were performed in running buffer consisting of 5% DMSO in PBS-P20 (GE). Evaluation version 3.1 software provided by Biacore and the 1:1 Langmuir combined model were employed for data analysis.

Mouse infection model

For the acute toxicity model, after pretreatment of TcdB with CAPE (2 or 4 μg/mL) for 1 h, the mice were intraperitoneally injected with a complex of TcdB-solvent or TcdB-CAPE (30 ng of TcdB per mouse). The survival of mice was observed for 72 h.

For the CDI model, mice were given cefoperazone (0.5 g/L) in their drinking water for 5 days (from day -7 to day -2), followed by switching to sterilized water for 2 days. On day 0, the mice were challenged with 1×10^8 colony-forming units (CFUs) of *C. difficile* BAA-1870 (Ribotype 027) by oral gavage. For the CAPE or melatonin treatment group, mice were treated with

CAPE (30 mg/kg by oral gavage) or melatonin (200 mg/kg by oral gavage) every day after *C. difficile* challenge. The weight loss and fecal state of the mice were monitored daily. Fecal samples were collected on days 0-3 to evaluate the stool water content as a marker of diarrhea. Additionally, fecal samples on day 3 were collected to assess *C. difficile* colonization. Colonic tissues were collected on day 3 post infection, stained with hematoxylin and eosin (H&E) and scored as previously described [66].

Fecal samples were collected on day 3 post infection, frozen in liquid nitrogen and transferred to the laboratory with dry ice for 16S rRNA sequencing and untargeted metabolomics analysis (Novogene Bioinformatics Technology Co., Ltd., Tianjin, China). The melatonin level in mouse stool supernatant was determined using the Mouse MT (Melatonin) ELISA Kit (Sangon Biotechnology Co., Ltd., Shanghai, China).

Statistical analysis

Western blot densitometry and LysoTracker fluorescence intensity were measured using ImageJ software (NIH, Bethesda, MD, USA). Statistical analysis was performed using GraphPad Prism 9.0 (GraphPad Software, USA). Unpaired two-tailed Student's t tests were used for comparing two groups, and one-way analysis of variance (ANOVA) was used for analyzing data from more than three groups. The statistical significance was determined using the log-rank (Mantel–Cox) test (survival rates) and Mann–Whitney U test (tissue bacterial load) *in vivo*. All the data are expressed as the mean ± standard

deviation (SD). * indicates $p < 0.05$ and ** indicates $p < 0.01$.

Acknowledgments

The authors thank Professor Aiwu Wu (Guangzhou Medical University) for the *C. difficile* BAA-1870 strain and Professor Hanping Feng (Tufts University) for the pHis1522-TcdB plasmid. This work was supported by the National Key Research & Development Program of China (2021YFD1801000), National Natural Science Foundation of China (32200141), the Natural Science Foundation of Jilin Province (20230101142JC and 20240101282JC), and The Fundamental Research Funds for the Central Universities.

Author contributions

Y.G., L.Q.H and J.Z.Q designed the study and wrote the manuscript. Y.G., Y.Z., G.Z.W. and H.T.L. conducted experiments. J.F.W., X.M.D., L.Q.H. and J.Z.Q. supervised the study and revised the manuscript. All authors read and approved the final manuscript. J.Z.Q. and L.Q.H. are responsible for the overall content as the guarantor.

Competing interests

The authors declare that they have no competing interests.

Data availability

All 16S rRNA gene sequencing data generated and analyzed during the current study were deposited in the Sequence Read Archive (SRA) under the BioProject accession number PRJNA1100298. Untargeted metabolomics data are available via Metabolights with the identifier MTBLS9938.

References

1. Smits WK, Lyras D, Lacy DB, Wilcox MH, Kuijper EJ. Clostridium difficile infection. *Nat Rev Dis Primers* **2**, 16020 (2016).

2. Miller BA, Chen LF, Sexton DJ, Anderson DJ. Comparison of the burdens of hospital-onset, healthcare facility-associated Clostridium difficile Infection and of healthcare-associated infection due to methicillin-resistant Staphylococcus aureus in community hospitals. *Infect Control Hosp Epidemiol* **32**, 387-390 (2011).

3. Kelly CP, LaMont JT. Clostridium difficile--more difficult than ever. *N Engl J Med* **359**, 1932-1940 (2008).

4. Dubberke E. Clostridium difficile infection: the scope of the problem. *J Hosp Med* **7 Suppl 3**, S1-4 (2012).

5. Lessa FC*, et al.* Burden of Clostridium difficile infection in the United States. *N Engl J Med* **372**, 825-834 (2015).

6. Goorhuis A*, et al.* Emergence of Clostridium difficile infection due to a new hypervirulent strain, polymerase chain reaction ribotype 078. *Clin Infect Dis* **47**, 1162-1170 (2008).

7. He M*, et al.* Emergence and global spread of epidemic healthcare-associated Clostridium difficile. *Nat Genet* **45**, 109-113 (2013).

8. Clements AC, Magalhaes RJ, Tatem AJ, Paterson DL, Riley TV. Clostridium difficile PCR ribotype 027: assessing the risks of further worldwide spread. *Lancet Infect Dis* **10**, 395-404 (2010).

9. Cornely OA*, et al.* Fidaxomicin versus vancomycin for infection with Clostridium difficile in Europe, Canada, and the USA: a double-blind, non-inferiority, randomised controlled trial. *Lancet Infect Dis* **12**, 281-289 (2012).

10. Bingley PJ, Harding GM. Clostridium difficile colitis following treatment with metronidazole and vancomycin. *Postgrad Med J* **63**, 993-994 (1987).

11. Feuerstadt P, Theriault N, Tillotson G. The burden of CDI in the United States: a multifactorial challenge. *BMC Infect Dis* **23**, 132 (2023).

12. Hopkins RJ, Wilson RB. Treatment of recurrent Clostridium difficile colitis: a narrative review. *Gastroenterol Rep (Oxf)* **6**, 21-28 (2018).

13. Spigaglia P, Mastrantonio P, Barbanti F. Antibiotic Resistances of Clostridium difficile. *Adv Exp Med Biol* **1050**, 137-159 (2018).

14. Seekatz AM, Young VB. Clostridium difficile and the microbiota. *J Clin Invest* **124**, 4182-4189 (2014).

15. Paredes-Sabja D, Shen A, Sorg JA. Clostridium difficile spore biology: sporulation, germination, and spore structural proteins. *Trends Microbiol* **22**, 406-416 (2014).

16. Lyras D*, et al.* Toxin B is essential for virulence of Clostridium difficile. *Nature* **458**, 1176-1179 (2009).

17. Kuehne SA, Cartman ST, Heap JT, Kelly ML, Cockayne A, Minton NP. The role of toxin A and toxin B in Clostridium difficile infection. *Nature* **467**, 711-713 (2010).

18. Carter GP*, et al.* Defining the Roles of TcdA and TcdB in Localized Gastrointestinal Disease, Systemic Organ Damage, and the Host Response during Clostridium difficile Infections. *mBio* **6**, e00551 (2015).

19. Drudy D, Fanning S, Kyne L. Toxin A-negative, toxin B-positive Clostridium difficile. *Int J Infect Dis* **11**, 5-10 (2007).

20. Chen P*, et al.* Structure of the full-length Clostridium difficile toxin B. *Nat Struct Mol Biol* **26**, 712-719 (2019).

21. Orrell KE, Melnyk RA. Large Clostridial Toxins: Mechanisms and Roles in Disease. *Microbiol Mol Biol Rev* **85**, e0006421 (2021).

22. Rasko DA, Sperandio V. Anti-virulence strategies to combat bacteria-mediated disease. *Nat Rev Drug Discov* **9**, 117-128 (2010).

23. Tam J, Beilhartz GL, Auger A, Gupta P, Therien AG, Melnyk RA. Small molecule inhibitors of Clostridium difficile toxin B-induced cellular damage. *Chem Biol* **22**, 175-185 (2015).

24. Balaha M, De Filippis B, Cataldi A, di Giacomo V. CAPE and Neuroprotection: A Review. *Biomolecules* **11**, (2021).

25. Garland M*, et al.* The Clinical Drug Ebselen Attenuates Inflammation

and Promotes Microbiome Recovery in Mice after Antibiotic Treatment for CDI. *Cell Rep Med* **1**, (2020).

26. Li X*, et al.* A strain of Bacteroides thetaiotaomicron attenuates colonization of Clostridioides difficile and affects intestinal microbiota and bile acids profile in a mouse model. *Biomed Pharmacother* **137**, 111290 (2021).

27. Kienesberger B*, et al.* (S)-Reutericyclin: Susceptibility Testing and In Vivo Effect on Murine Fecal Microbiome and Volatile Organic Compounds. *Int J Mol Sci* **22**, (2021).

28. Khanna S*, et al.* Gut microbiome predictors of treatment response and recurrence in primary Clostridium difficile infection. *Aliment Pharmacol Ther* **44**, 715-727 (2016).

29. Dong D*, et al.* Effects of intestinal colonization by Clostridium difficile and Staphylococcus aureus on microbiota diversity in healthy individuals in China. *BMC Infect Dis* **18**, 207 (2018).

30. Gurung B, Stricklin M, Wang S. Gut Microbiota-Gut Metabolites and Clostridioides difficile Infection: Approaching Sustainable Solutions for Therapy. *Metabolites* **14**, (2024).

31. Cronstein BN. Adenosine, an endogenous anti-inflammatory agent. *J Appl Physiol (1985)* **76**, 5-13 (1994).

32. Yong T*, et al.* Caffeic acid phenethyl ester alleviated hypouricemia in hyperuricemic mice through inhibiting XOD and up-regulating OAT3. *Phytomedicine* **103**, 154256 (2022).

33. de Araujo Junqueira AF*, et al.* Adenosine deaminase inhibition prevents Clostridium difficile toxin A-induced enteritis in mice. *Infect Immun* **79**, 653-662 (2011).

34. Neumann-Schaal M, Jahn D, Schmidt-Hohagen K. Metabolism the Difficile Way: The Key to the Success of the Pathogen Clostridioides difficile. *Front Microbiol* **10**, 219 (2019).

35. Bouillaut L, Self WT, Sonenshein AL. Proline-dependent regulation of Clostridium difficile Stickland metabolism. *J Bacteriol* **195**, 844-854 (2013).

36. Jackson S, Calos M, Myers A, Self WT. Analysis of proline reduction in

the nosocomial pathogen Clostridium difficile. *J Bacteriol* **188**, 8487-8495 (2006).

37. Sutton SS, Magagnoli J, Cummings TH, Hardin JW. Melatonin as an Antimicrobial Adjuvant and Anti-Inflammatory for the Management of Recurrent Clostridioides difficile Infection. *Antibiotics (Basel)* **11**, (2022).

38. 2019 AR Threats Report., 2019. [Available from: https://www.cdc.gov/drugresistance/biggest-threats.html].

39. Abbas A, Zackular JP. Microbe-microbe interactions during Clostridioides difficile infection. *Curr Opin Microbiol* **53**, 19-25 (2020).

40. Raplee I*, et al.* Emergence of nosocomial associated opportunistic pathogens in the gut microbiome after antibiotic treatment. *Antimicrob Resist Infect Control* **10**, 36 (2021).

41. Beilhartz GL, Tam J, Melnyk RA. Small Molecules Take A Big Step Against Clostridium difficile. *Trends Microbiol* **23**, 746-748 (2015).

42. Ranftler C*, et al.* Binding and neutralization of C. difficile toxins A and B by purified clinoptilolite-tuff. *PLoS One* **16**, e0252211 (2021).

43. Zucca M, Scutera S, Savoia D. Novel avenues for Clostridium difficile infection drug discovery. *Expert Opin Drug Discov* **8**, 459-477 (2013).

44. Kuehne SA, Collery MM, Kelly ML, Cartman ST, Cockayne A, Minton NP. Importance of toxin A, toxin B, and CDT in virulence of an epidemic Clostridium difficile strain. *J Infect Dis* **209**, 83-86 (2014).

45. Warny M*, et al.* Toxin production by an emerging strain of Clostridium difficile associated with outbreaks of severe disease in North America and Europe. *Lancet* **366**, 1079-1084 (2005).

46. Stewart D, Anwar F, Vedantam G. Anti-virulence strategies for Clostridioides difficile infection: advances and roadblocks. *Gut Microbes* **12**, 1802865 (2020).

47. Deeks ED. Bezlotoxumab: A Review in Preventing Clostridium difficile Infection Recurrence. *Drugs* **77**, 1657-1663 (2017).

48. Bender KO*, et al.* A small-molecule antivirulence agent for treating Clostridium difficile infection. *Sci Transl Med* **7**, 306ra148 (2015).

49. Chan H*, et al.* Vitamin D(3) and carbamazepine protect against Clostridioides difficile infection in mice by restoring macrophage lysosome acidification. *Autophagy* **18**, 2050-2067 (2022).

50. Tam J*, et al.* Host-targeted niclosamide inhibits C. difficile virulence and prevents disease in mice without disrupting the gut microbiota. *Nat Commun* **9**, 5233 (2018).

51. Tam J*, et al.* Intestinal bile acids directly modulate the structure and function of C. difficile TcdB toxin. *Proc Natl Acad Sci U S A* **117**, 6792-6800 (2020).

52. Tek NA, Senture SA, Ersoy N. Is Propolis a Potential Anti-Obesogenic Agent for Obesity? *Curr Nutr Rep*, (2024).

53. Schubert AM, Sinani H, Schloss PD. Antibiotic-Induced Alterations of the Murine Gut Microbiota and Subsequent Effects on Colonization Resistance against Clostridium difficile. *mBio* **6**, e00974 (2015).

54. van Nood E*, et al.* Duodenal infusion of donor feces for recurrent Clostridium difficile. *N Engl J Med* **368**, 407-415 (2013).

55. Bornet E, Westermann AJ. The ambivalent role of Bacteroides in enteric infections. *Trends Microbiol* **30**, 104-108 (2022).

56. Pike CM, Theriot CM. Mechanisms of Colonization Resistance Against Clostridioides difficile. *J Infect Dis* **223**, S194-S200 (2021).

57. Deng H*, et al.* Corrigendum: Bacteroides fragilis Prevents Clostridium difficile Infection in a Mouse Model by Restoring Gut Barrier and Microbiome Regulation. *Front Microbiol* **10**, 601 (2019).

58. Lee C*, et al.* Safety of fecal microbiota, live-jslm (REBYOTA()) in individuals with recurrent Clostridioides difficile infection: data from five prospective clinical trials. *Therap Adv Gastroenterol* **16**, 17562848231174277 (2023).

59. Gonzales-Luna AJ, Carlson TJ, Garey KW. Review Article: Safety of Live Biotherapeutic Products Used for the Prevention of Clostridioides difficile Infection Recurrence. *Clin Infect Dis* **77**, S487-S496 (2023).

60. Hasko G, Linden J, Cronstein B, Pacher P. Adenosine receptors: therapeutic aspects for inflammatory and immune diseases. Nat Rev

Drug Discov 7, 759-770 (2008).

61. Shakya AK, Naik RR, Almasri IM, Kaur A. Role and Function of Adenosine and its Receptors in Inflammation, Neuroinflammation, IBS, Autoimmune Inflammatory Disorders, Rheumatoid Arthritis and Psoriasis. Curr Pharm Des 25, 2875-2891 (2019).

62. Cavalcante IC*, et al.* Effect of novel A2A adenosine receptor agonist ATL 313 on Clostridium difficile toxin A-induced murine ileal enteritis. *Infect Immun* **74**, 2606-2612 (2006).

63. Ma N, Zhang J, Reiter RJ, Ma X. Melatonin mediates mucosal immune cells, microbial metabolism, and rhythm crosstalk: A therapeutic target to reduce intestinal inflammation. *Med Res Rev* **40**, 606-632 (2020).

64. Yang G*, et al.* Expression of recombinant Clostridium difficile toxin A and B in Bacillus megaterium. *BMC Microbiol* **8**, 192 (2008).

65. Fletcher JR*, et al.* Clostridioides difficile exploits toxin-mediated inflammation to alter the host nutritional landscape and exclude competitors from the gut microbiota. *Nat Commun* **12**, 462 (2021).

66. Reeves AE, Theriot CM, Bergin IL, Huffnagle GB, Schloss PD, Young VB. The interplay between microbiome dynamics and pathogen dynamics in a murine model of Clostridium difficile Infection. *Gut Microbes* **2**, 145-158 (2011).

Figures

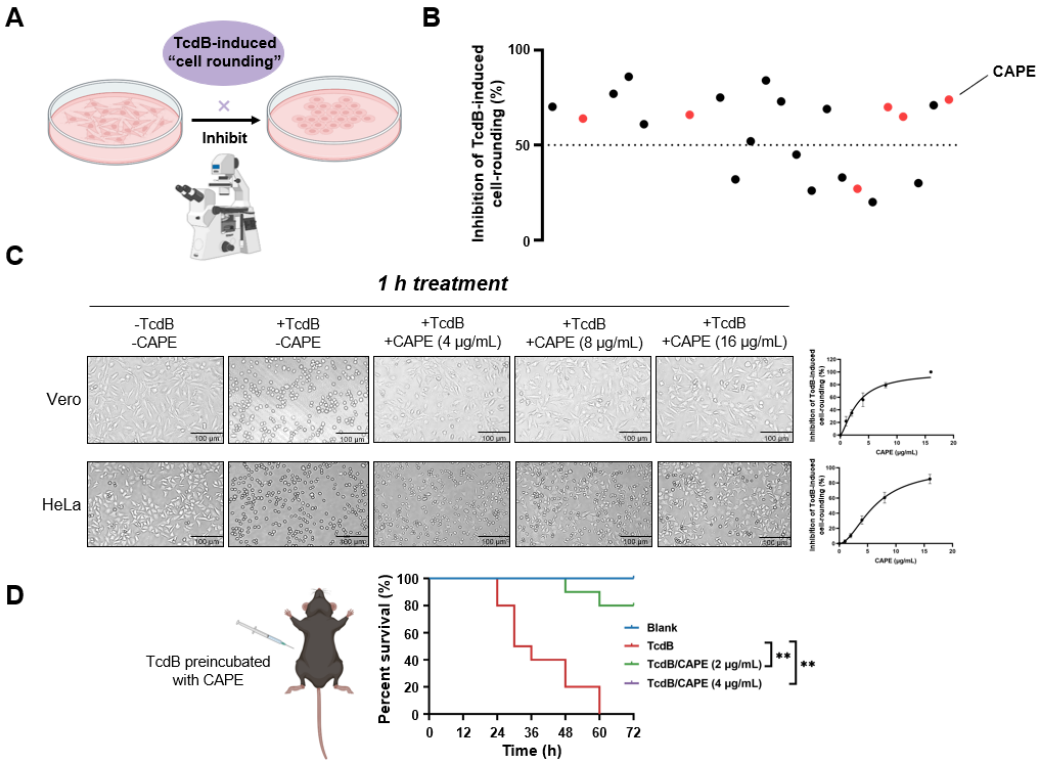

Figure 1. CAPE suppresses TcdB-mediated cell rounding.

(A) Schematic of the process used for the identification of small molecules that inhibit the cell rounding phenotype induced by TcdB. TcdB (0.2 ng/mL) was preincubated with 8 μg/mL of individual compounds prior to addition to the cell cultures. **(B)** Active compounds were identified from the chemical library consisting of 2076 chemicals. The red dots represent caffeic acid and its derivatives. **(C)** Dose-dependent CAPE inhibition of TcdB-induced rounding of Vero (upper) and HeLa (lower) cells. Scale bar, 100 μm. The dose titration curves are presented on the right. **(D)** The survival rates of mice that were intraperitoneally injected with CAPE-pretreated or native TcdB (30 ng). * p <0.05 and ** p <0.01 by log-rank (Mantel□Cox) test.

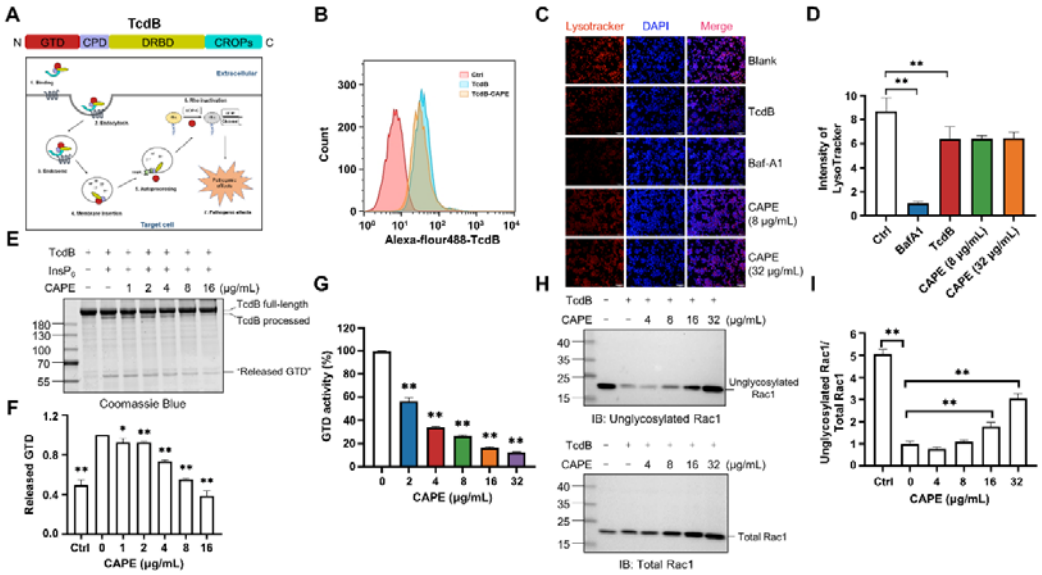

Figure 2. Mechanism by which CAPE suppresses TcdB intoxication.

(A) Schematic illustration of the multistep mechanism of TcdB intoxication of host cells. **(B)** Determination of internalized TcdB levels. Alexa Fluor 488-labeled TcdB was incubated with 32 μg/mL CAPE for 30 min before it was added to the cell culture. The cellular uptake of TcdB was measured by flow cytometry analysis. **(C)** Lysosomal activity in host cells treated with CAPE was measured via LysoTracker staining. The nuclei were stained with DAPI. Bar, 100 μm. **(D)** The intensities of LysoTracker staining were quantified using ImageJ. * p <0.05; ** p <0.01 using one-way ANOVA. **(E-F)** CAPE inhibits $InsP_6$-induced autoprocessing of full-length TcdB. Two micrograms of TcdB was preincubated with increasing concentrations of CAPE for 1 h. Self-cleavage of TcdB was initiated by the addition of 3 μg of $InsP_6$ and the cells were incubated for 6 h at 37 ^{o}C. Reactions were terminated with 5x SDS loading buffer, and the release of GTD was visualized by CBB staining of the

SDS PAGE gel **(E)**. The level of released GTD in panel E was quantified by ImageJ **(F)** * p <0.05; ** p <0.01 using one-way ANOVA. **(G)** Dose-dependent inhibition of the GTD activity of TcdB by CAPE. Recombinant GTD of TcdB was mixed with different concentrations of CAPE (0-32 μg/mL) and incubated for 15 min at 25 ^{o}C. GTD activity was measured by the UDP-Glo™ glycosyltransferase assay. **(H-I)** Intracellular Rac1 glucosylation in cells treated with TcdB. Native or CAPE-pretreated TcdB was added to the cell culture and cells were incubated for 2 h. The cells were lysed, and the glucosylation of Rac1 was analyzed by western blotting using antibodies recognizing total Rac1 and unglycosylated Rac1 **(H)**. The level of Rac1 glucosylation shown in H was quantified by ImageJ **(I)**. * p <0.05; ** p <0.01 using one-way ANOVA.

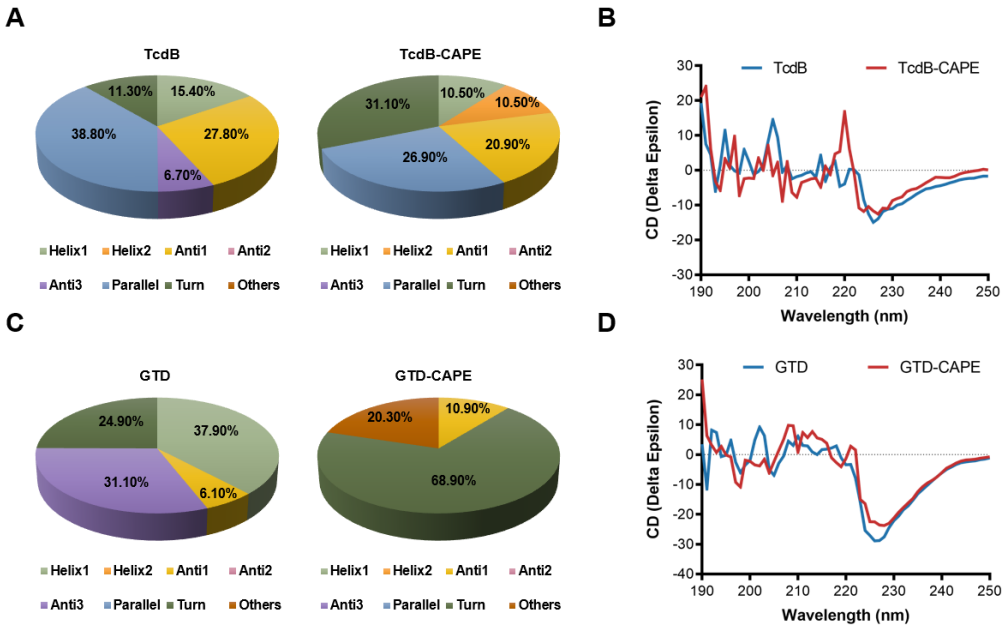

Figure 3. CAPE alters the secondary structure of TcdB and GTD.

(A-B) The secondary structure of TcdB **(A)** or GTD **(B)** in the presence or absence of 32 μg/mL CAPE was determined by CD spectroscopy. **(C-D)** Calculated CD spectra of CAPE-treated TcdB **(C)** and GTD **(D)**. The wavelength for CD spectroscopy was set at 190-250 nm.

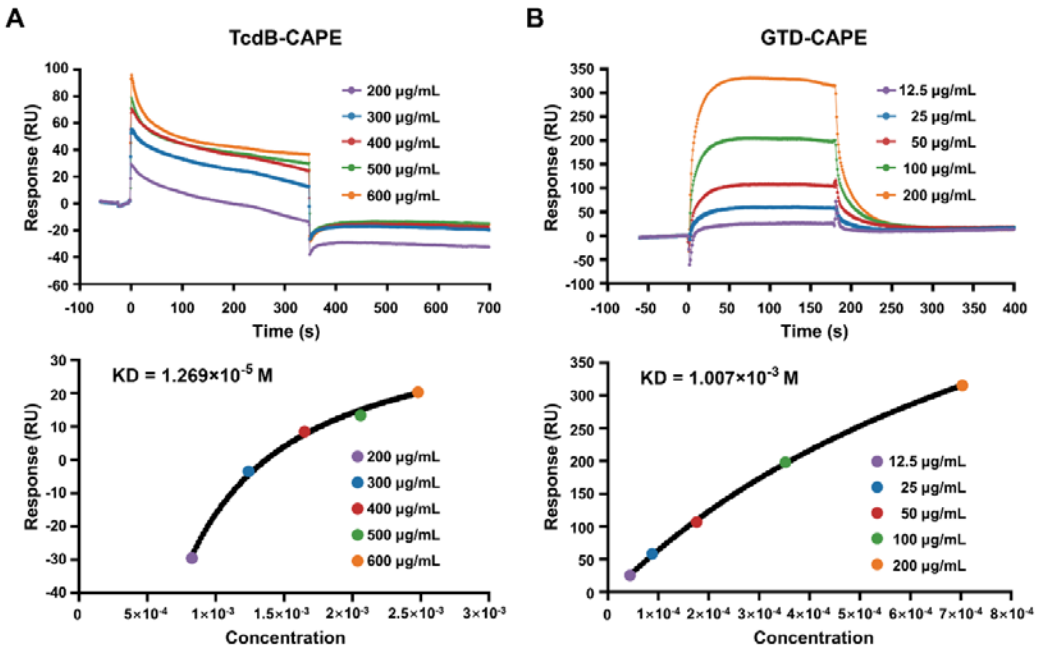

Figure 4. Direct interaction of CAPE with TcdB and GTD.

(A-B) Full-length TcdB or GTD was immobilized on a CM5 chip, followed by the injection of various concentrations of CAPE. The response unit (RU) value and affinities of CAPE interactions with TcdB **(A)** and GTD **(B)** were determined by a Biacore T100.

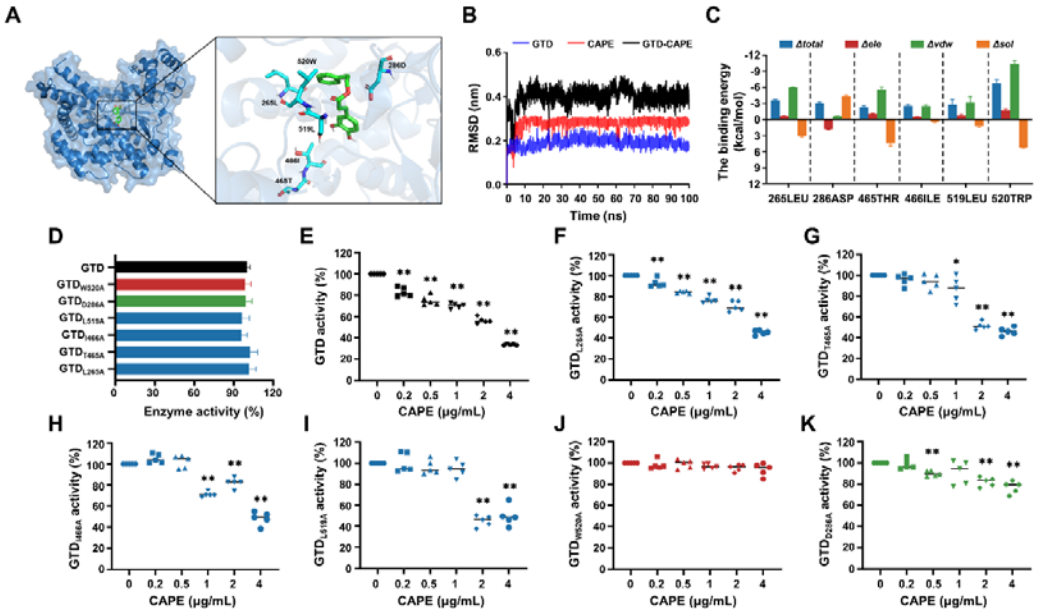

Figure 5. Asp286 and Trp520 in the GTD are critical for CAPE-mediated inhibition of GTD.

(A) Three-dimensional structure determination of GTD with the CAPE complex was performed by molecular modeling. **(B)** The RMSD values of the GTD-CAPE complex. **(C)** Decomposition of the binding energy on a per-residue basis in the binding sites of the GTD-CAPE complex. **(D)** Glucosyltransferase activity of wild-type GTD and the GTD mutants. **(E-K)** Residual activity of wild-type GTD **(E)** and its mutants GTD_{L265A} **(F)**, GTD_{T465A} **(G)**, GTD_{I466A} **(H)**, GTD_{L519A} **(I)**, GTD_{W520A} **(J)** and GTD_{D286A} **(K)** in the presence of increasing concentrations of CAPE (0-4 μg/mL). * p <0.05; ** p <0.01 using one-way ANOVA.

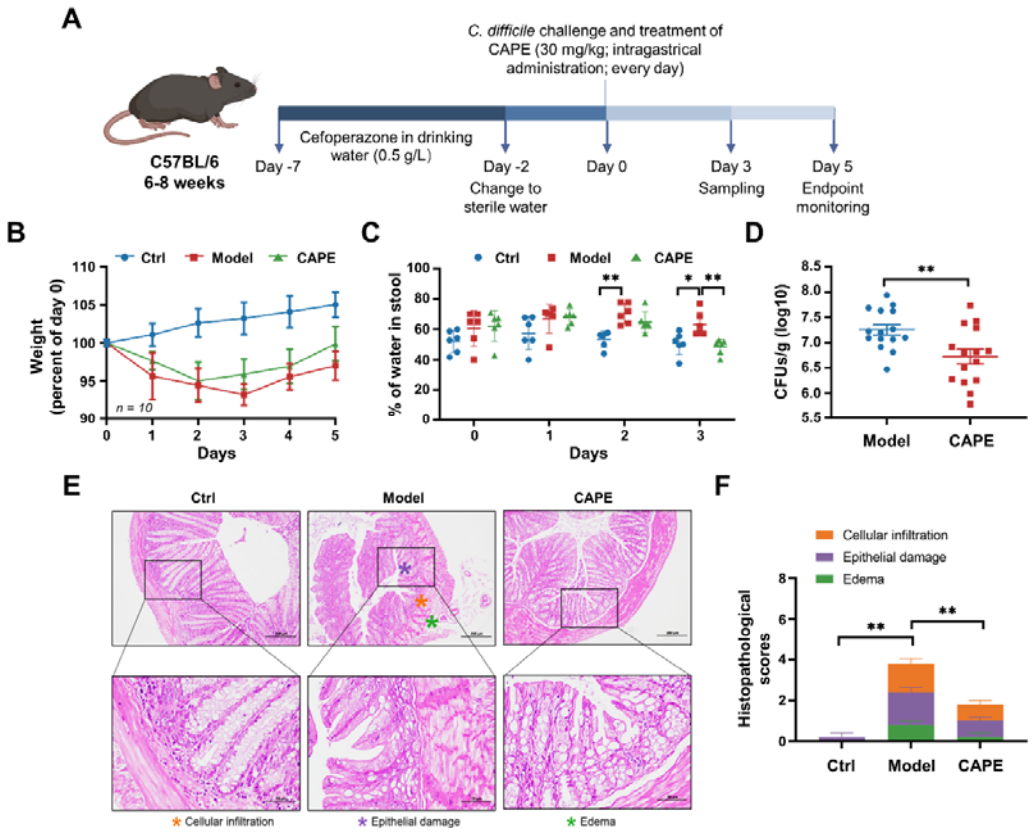

Figure 6. CAPE treatment blocks the pathology of CDI in mice.

(A) Schematic of the process used for the establishment of the CDI mouse model. **(B)** Weight changes in CDI mice after CAPE or vehicle treatment (n=10). **(C)** The fecal dry/wet weight ratio in CDI mice treated with CAPE or vehicle (n=6). * p <0.05; ** p <0.01 using one-way ANOVA. **(D)** Bacterial colonization in the feces of CDI mice treated with CAPE or vehicle (n=15). * p <0.05; ** p <0.01 using the Mann□Whitney U test. **(E)** Pathological analysis of colon sections from CDI mice treated with CAPE or vehicle. The black boxes are the regions that were magnified and are shown underneath. **(F)** Histopathological scores of vehicle-treated and CAPE-treated mice in terms of cell infiltration (orange), epithelial damage (purple), and edema (green). * p

<0.05; ** *p* <0.01 using one-way ANOVA.

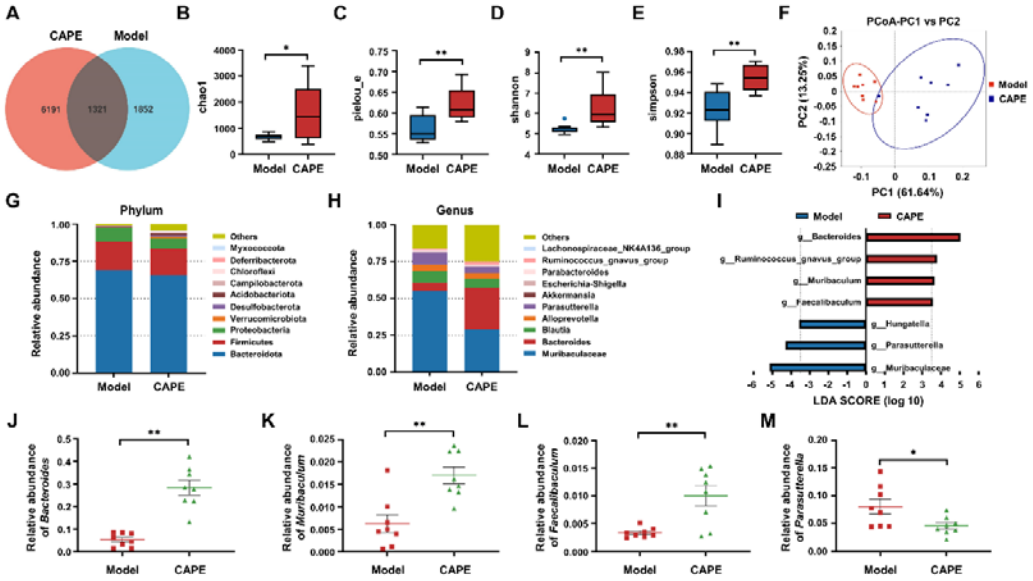

Figure 7. The influence of CAPE treatment on the diversity and composition of the gut microbiota in CDI mice.

(A) Venn diagram illustrating the numbers of differentially abundant bacteria identified using a single model and their cooperation. **(B-E)** Quantification of the α diversity of the gut microbiota according to the observed species richness **(B-C),** Shannon index **(D)**, and Simpson index **(E)**. **(F)** PCoA showing β diversity based on the weighted UniFrac distance. **(G-H)** Relative abundance of the top 10 predominant bacteria classified at the phylum **(G)** and genus **(H)** levels. **(I)** Significant changes in flora among the model and CAPE groups, as measured by LEfSe analysis (LDA score [log 10] > 3.5). **(J-M)** Relative abundances of *Bacteroides* **(J)**, *Muribaculum* **(K)**, *Faecalibaculum* **(L)**, and *Parasutterella* **(M)** in mice in the model and CAPE treatment groups. * p <0.05; ** p <0.01 using an unpaired Student's t test.

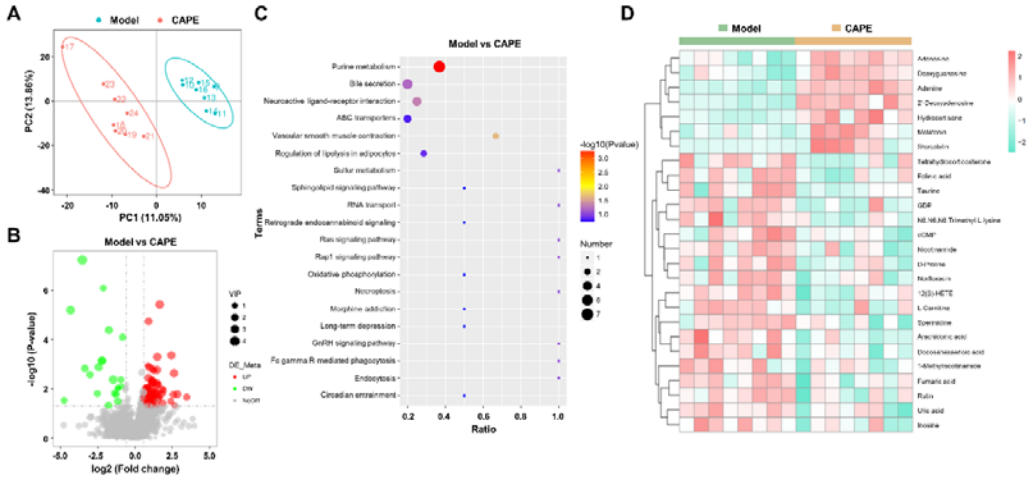

Figure 8. Alterations in gut metabolites in CAPE-treated mice with CDI. **(A)** The score plots show orthogonal partial least square discriminant analysis (PLS-DA) results. **(B)** Volcano plot representing the upregulated or downregulated gut metabolites in the CAPE treatment group compared to those in the model group. **(C)** Enrichment bubble map of the top 20 metabolic pathways in the CAPE treatment and model groups. **(D)** The 26 potential biomarkers are displayed in a heatmap, along with hierarchical clustering analysis.

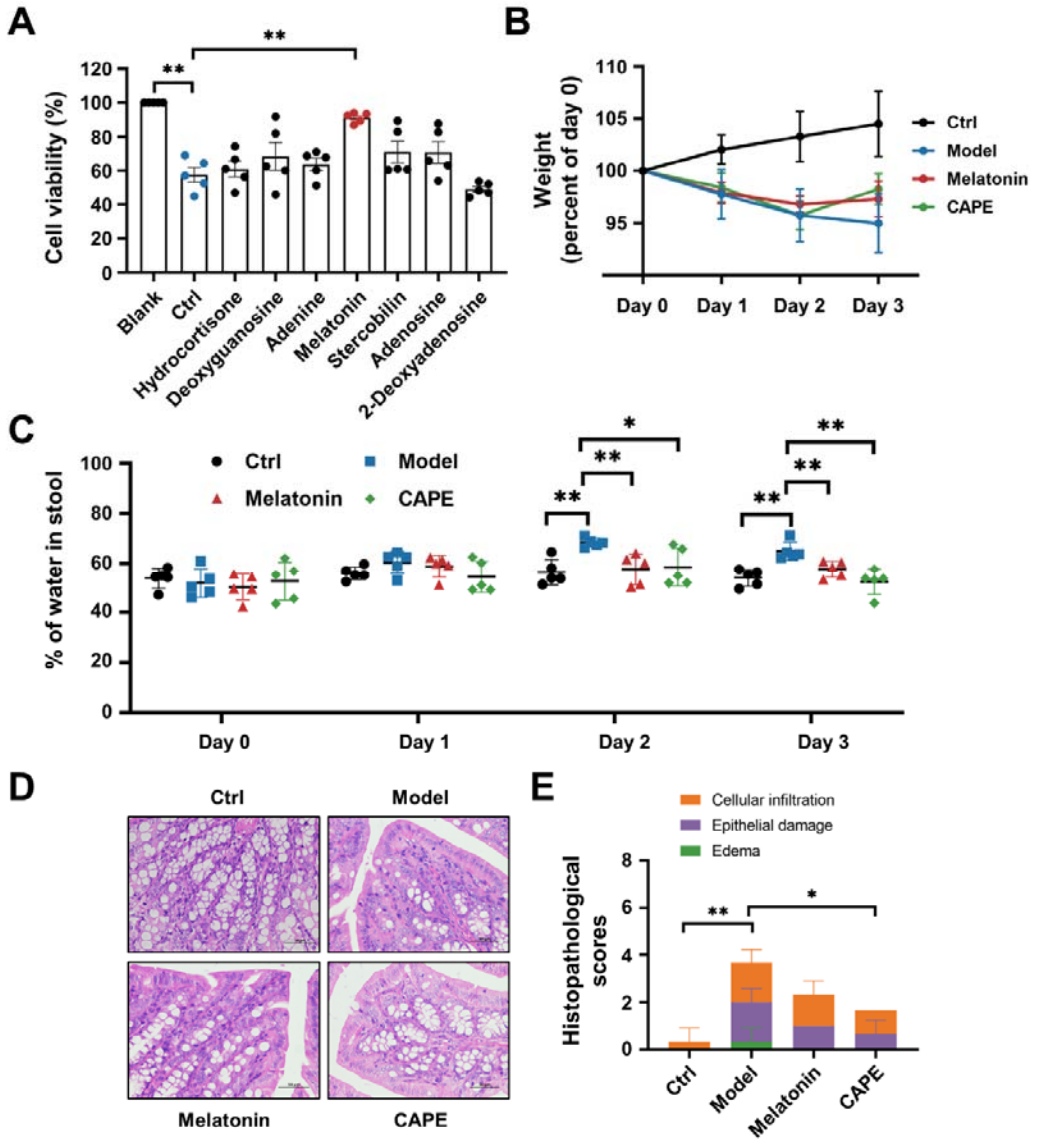

Figure 9. Oral administration of melatonin alleviates the pathology of CDI. **(A)** The impact of upregulated metabolites on the cytotoxicity of TcdB. TcdB (0.2 ng/mL) was incubated with each of the metabolites (100 μg/mL) for 1 h at 37 ^{o}C before being added to the Vero cell culture. At 3 h after TcdB treatment, cell death was evaluated with a CCK-8 kit. **(B)** Body weight changes in melatonin-treated CDI mice (n=5). **(C)** The fecal dry/wet weight ratio in CDI mice after melatonin treatment (n=5). **(D)** Histopathological analysis of colon

tissue from CDI mice treated with melatonin. **(E)** Histopathological scores of melatonin-treated CDI mice. * $p < 0.05$; ** $p < 0.01$ using one-way ANOVA.

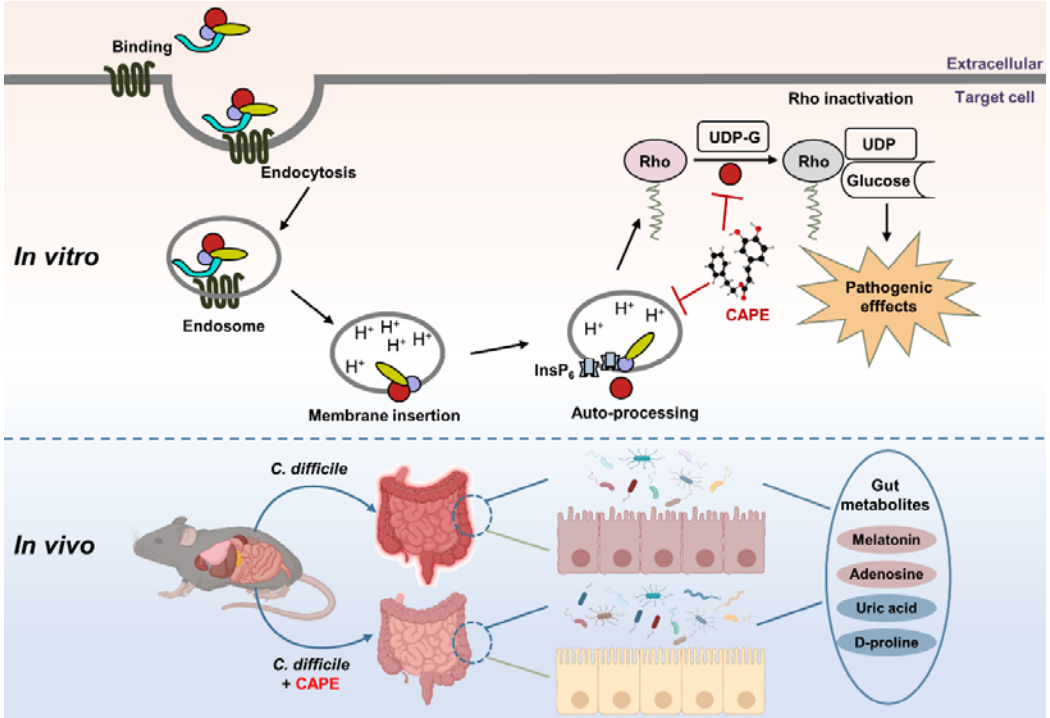

Figure 10. A model for CAPE-mediated suppression of TcdB cytotoxicity and protection of mice from CDI.

The intoxication of cells by TcdB involves multistep mechanisms. Direct interaction of CAPE with full-length TcdB blocks $InsP_6$-induced autoproteolysis, resulting in decreased production of active GTD. The binding between GTD and CAPE inhibits its glucosyltransferase activity, thus decreasing the glucosylation level of Rac1. CAPE treatment of CDI mice markedly restored the diversity and composition of the gut microbiota and induced changes in gut metabolites, which might have contributed to the therapeutic outcomes of CDI following CAPE treatment.

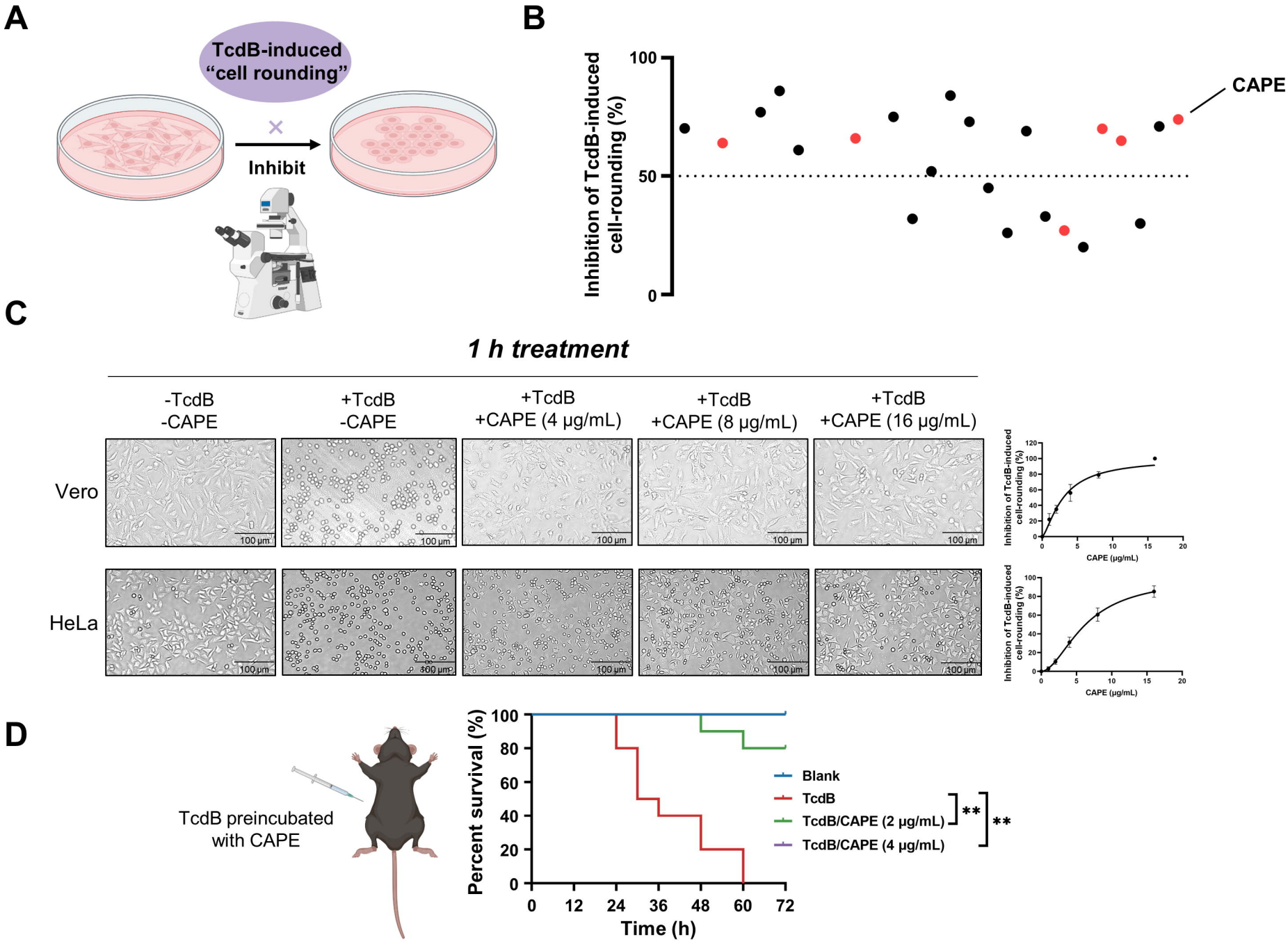
A
TcdB-induced
"cell rounding"
Inhibit
B
Inhibition of TcdB-induced cell-rounding (%)
100
50
0
CAPE
C
1 h treatment
-TcdB
-CAPE
+TcdB
-CAPE
+TcdB
+CAPE (4 μg/mL)
+TcdB
+CAPE (8 μg/mL)
+TcdB
+CAPE (16 μg/mL)
Vero
HeLa
100 μm
Inhibition of TcdB-induced cell-rounding (%)
CAPE (μg/mL)
D
TcdB preincubated
with CAPE
Percent survival (%)
Time (h)
Blank
TcdB
TcdB/CAPE (2 μg/mL)
TcdB/CAPE (4 μg/mL)
**
**

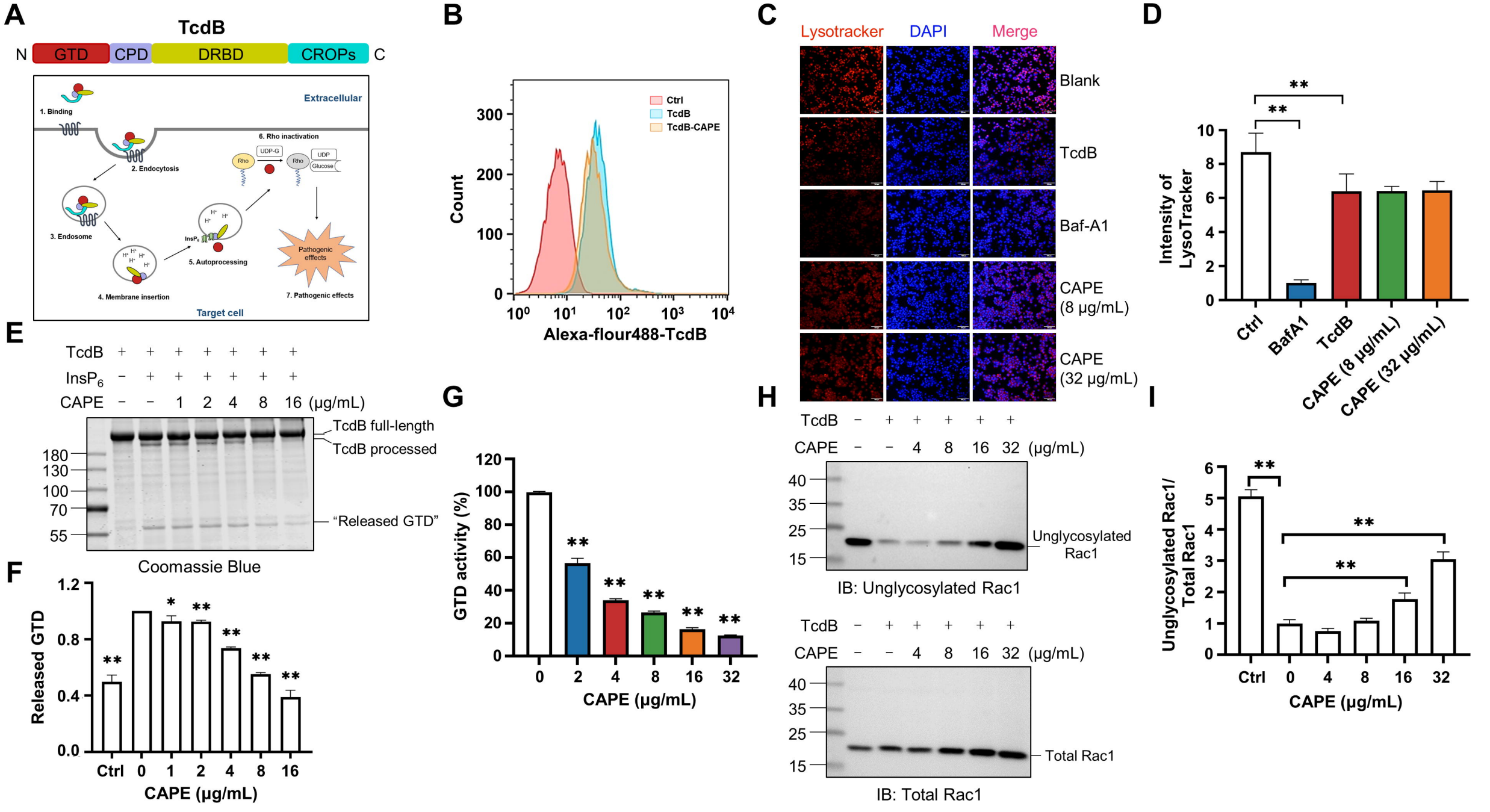
A
TcdB
N
GTD
CPD
DRBD
CROPs
C
Extracellular
1. Binding
2. Endocytosis
3. Endosome
4. Membrane insertion
5. Autoprocessing
6. Rho inactivation
UDP-G
UDP
Glucose
Rho
Pathogenic effects
7. Pathogenic effects
Target cell
B
Ctrl
TcdB
TcdB-CAPE
Count
Alexa-flour488-TcdB
C
Lysotracker
DAPI
Merge
Blank
TcdB
Baf-A1
CAPE (8 μg/mL)
CAPE (32 μg/mL)
D
Intensity of LysoTracker
Ctrl
BafA1
TcdB
CAPE (8 μg/mL)
CAPE (32 μg/mL)
E
TcdB
InsP6
CAPE (μg/mL)
TcdB full-length
TcdB processed
"Released GTD"
Coomassie Blue
F
Released GTD
CAPE (μg/mL)
G
GTD activity (%)
CAPE (μg/mL)
H
TcdB
CAPE (μg/mL)
Unglycosylated Rac1
IB: Unglycosylated Rac1
Total Rac1
IB: Total Rac1
I
Unglycosylated Rac1/ Total Rac1
CAPE (μg/mL)

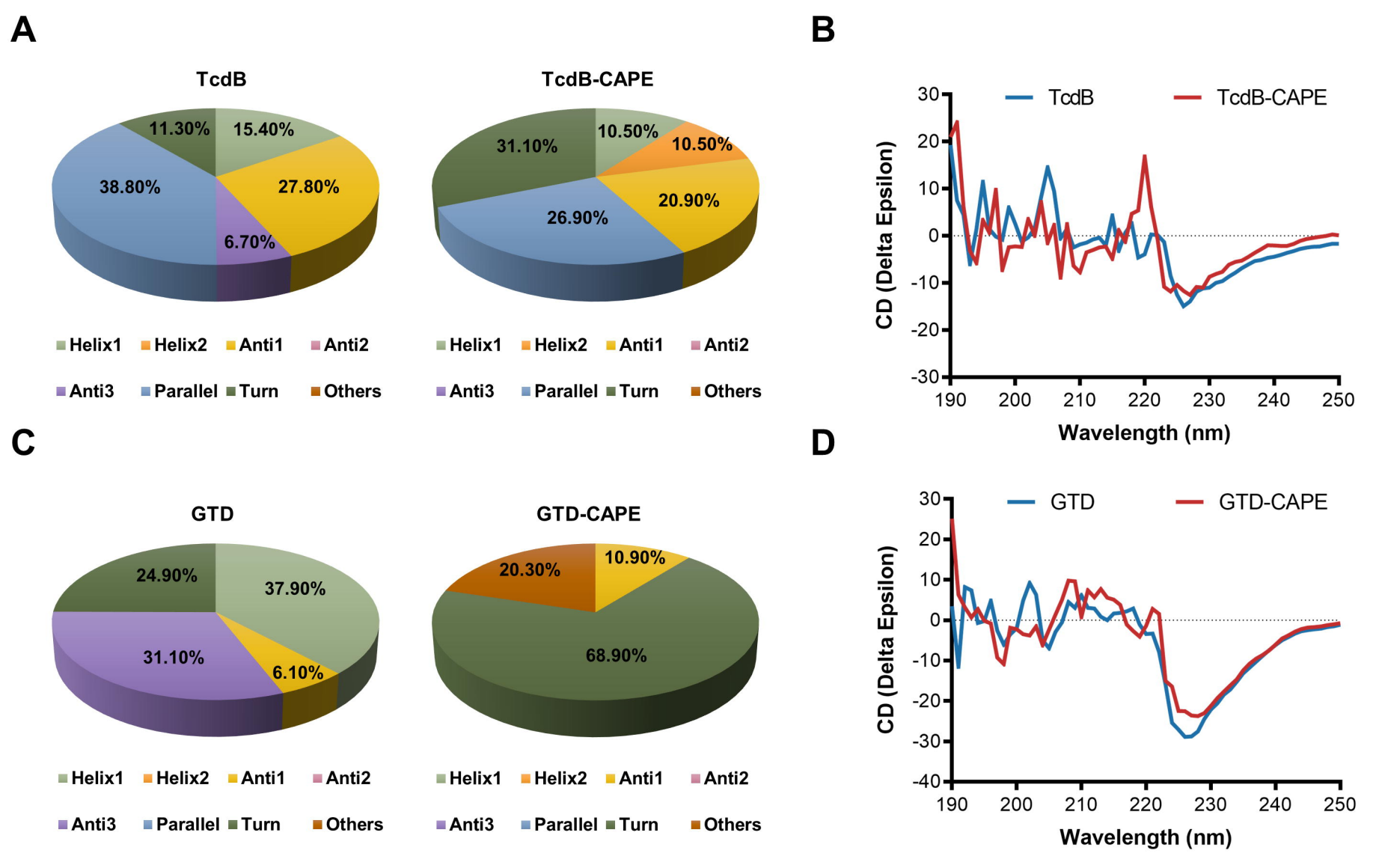
A
TcdB
11.30%
15.40%
38.80%
27.80%
6.70%
TcdB-CAPE
31.10%
10.50%
10.50%
20.90%
26.90%
Helix1
Helix2
Anti1
Anti2
Anti3
Parallel
Turn
Others
B
TcdB
TcdB-CAPE
CD (Delta Epsilon)
Wavelength (nm)
C
GTD
24.90%
37.90%
31.10%
6.10%
GTD-CAPE
20.30%
10.90%
68.90%
D
GTD
GTD-CAPE
CD (Delta Epsilon)
Wavelength (nm)

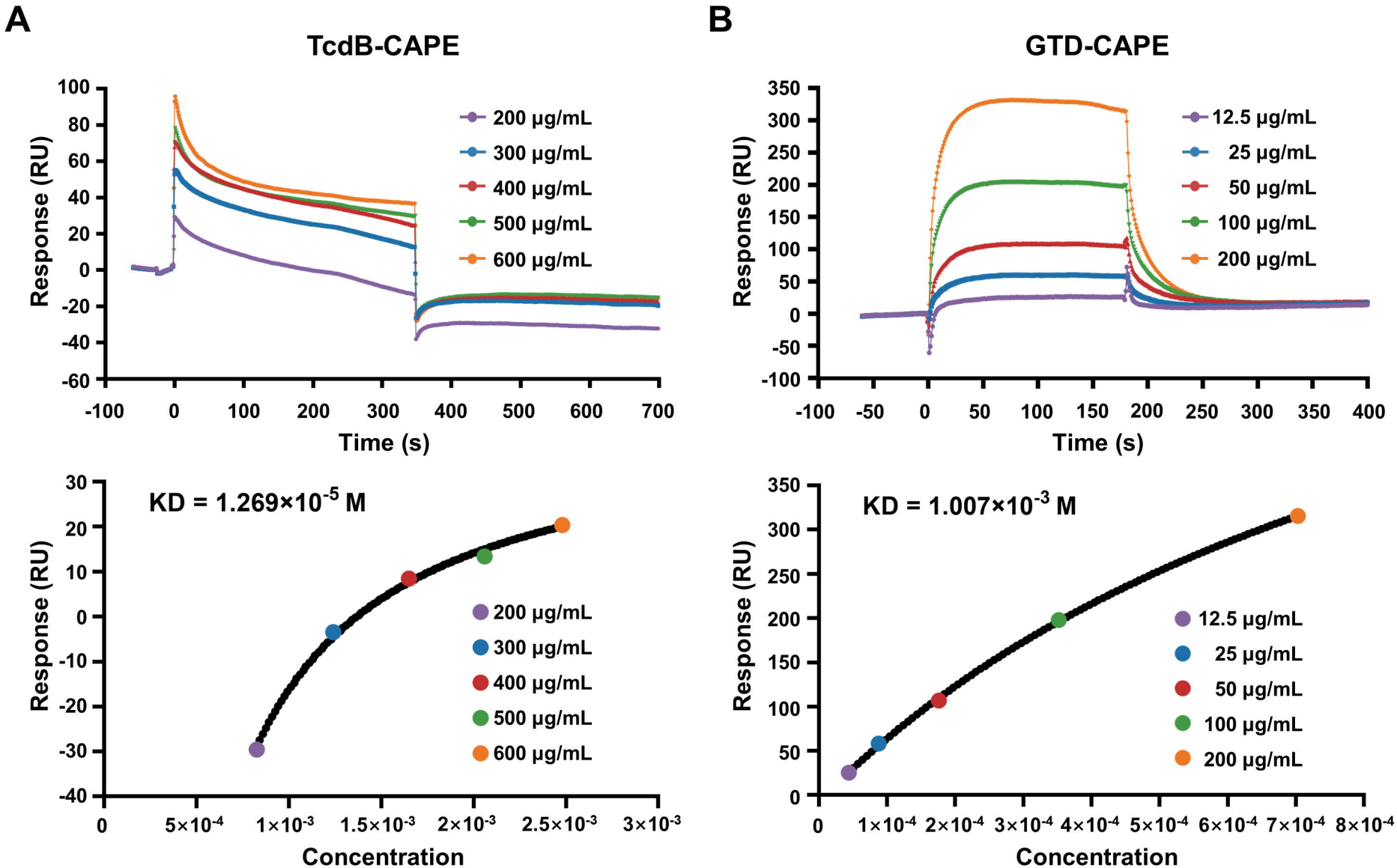
A
TcdB-CAPE
Response (RU)
Time (s)
200 μg/mL
300 μg/mL
400 μg/mL
500 μg/mL
600 μg/mL
KD = 1.269×10-5 M
Concentration
B
GTD-CAPE
Response (RU)
Time (s)
12.5 μg/mL
25 μg/mL
50 μg/mL
100 μg/mL
200 μg/mL
KD = 1.007×10-3 M
Concentration

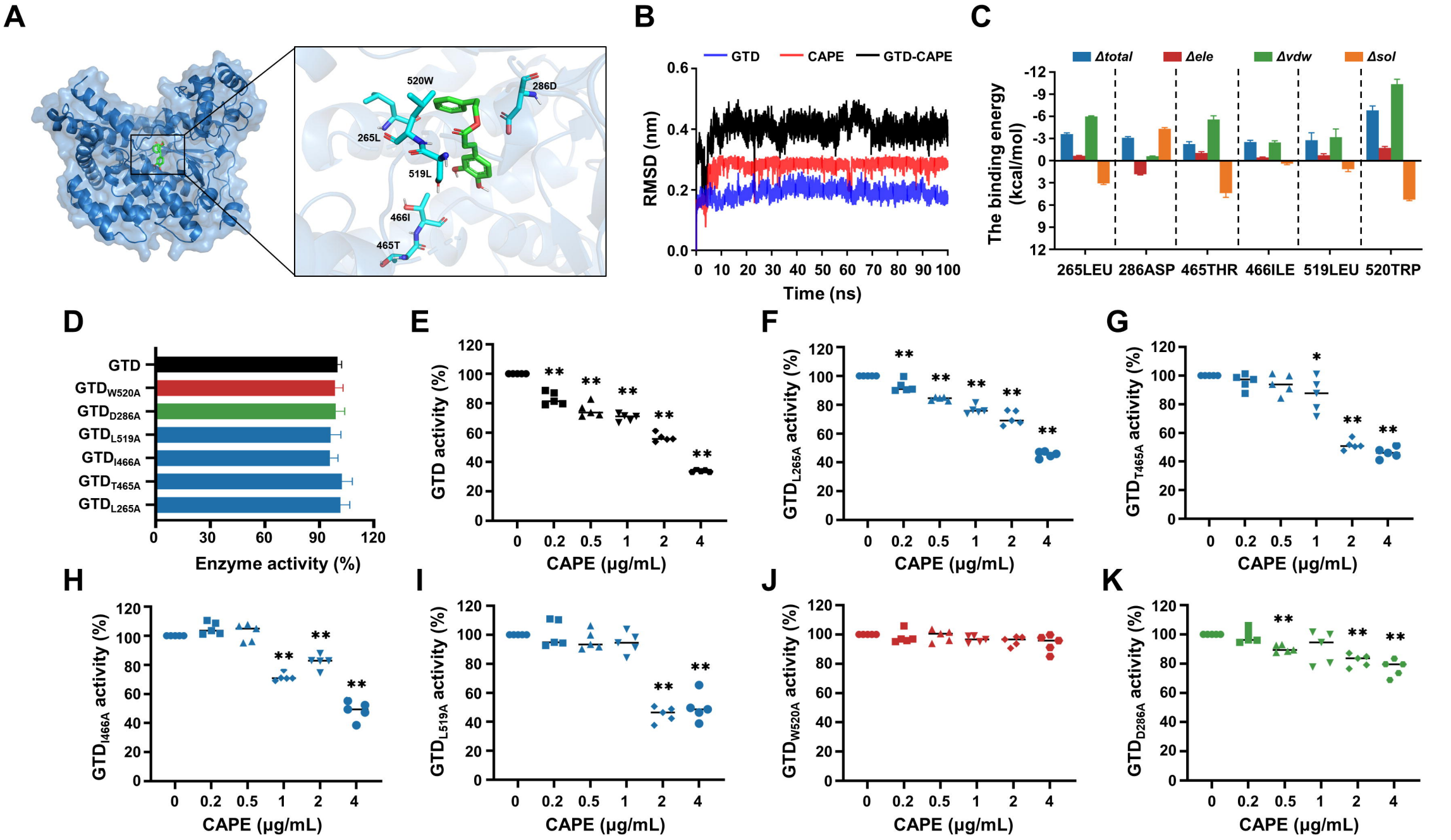
A
520W
286D
265L
519L
466I
465T
B
GTD
CAPE
GTD-CAPE
RMSD (nm)
Time (ns)
C
Δtotal
Δele
Δvdw
Δsol
The binding energy (kcal/mol)
265LEU
286ASP
465THR
466ILE
519LEU
520TRP
D
GTD
GTD W520A
GTD D286A
GTD L519A
GTD I466A
GTD T465A
GTD L265A
Enzyme activity (%)
E
GTD activity (%)
CAPE (μg/mL)
F
GTD L265A activity (%)
G
GTD T465A activity (%)
H
GTD I466A activity (%)
I
GTD L519A activity (%)
J
GTD W520A activity (%)
K
GTD D286A activity (%)

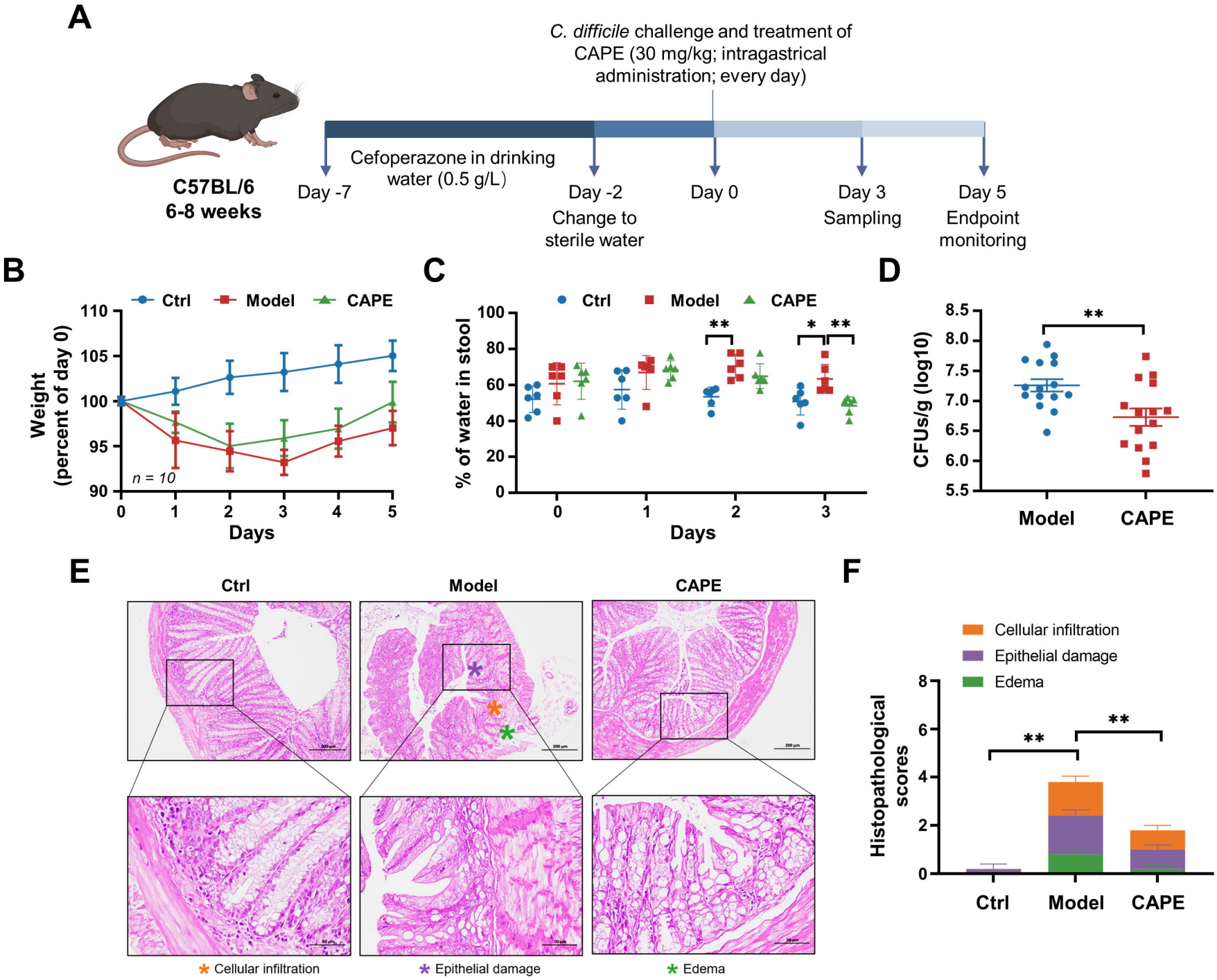
A
C. difficile challenge and treatment of CAPE (30 mg/kg; intragastrical administration; every day)
C57BL/6
6-8 weeks
Cefoperazone in drinking water (0.5 g/L)
Day -7
Day -2
Change to sterile water
Day 0
Day 3
Sampling
Day 5
Endpoint monitoring
B
Ctrl
Model
CAPE
Weight (percent of day 0)
n = 10
Days
C
% of water in stool
Days
D
CFUs/g (log10)
Model
CAPE
E
Ctrl
Model
CAPE
Cellular infiltration
Epithelial damage
Edema
F
Cellular infiltration
Epithelial damage
Edema
Histopathological scores
Ctrl
Model
CAPE

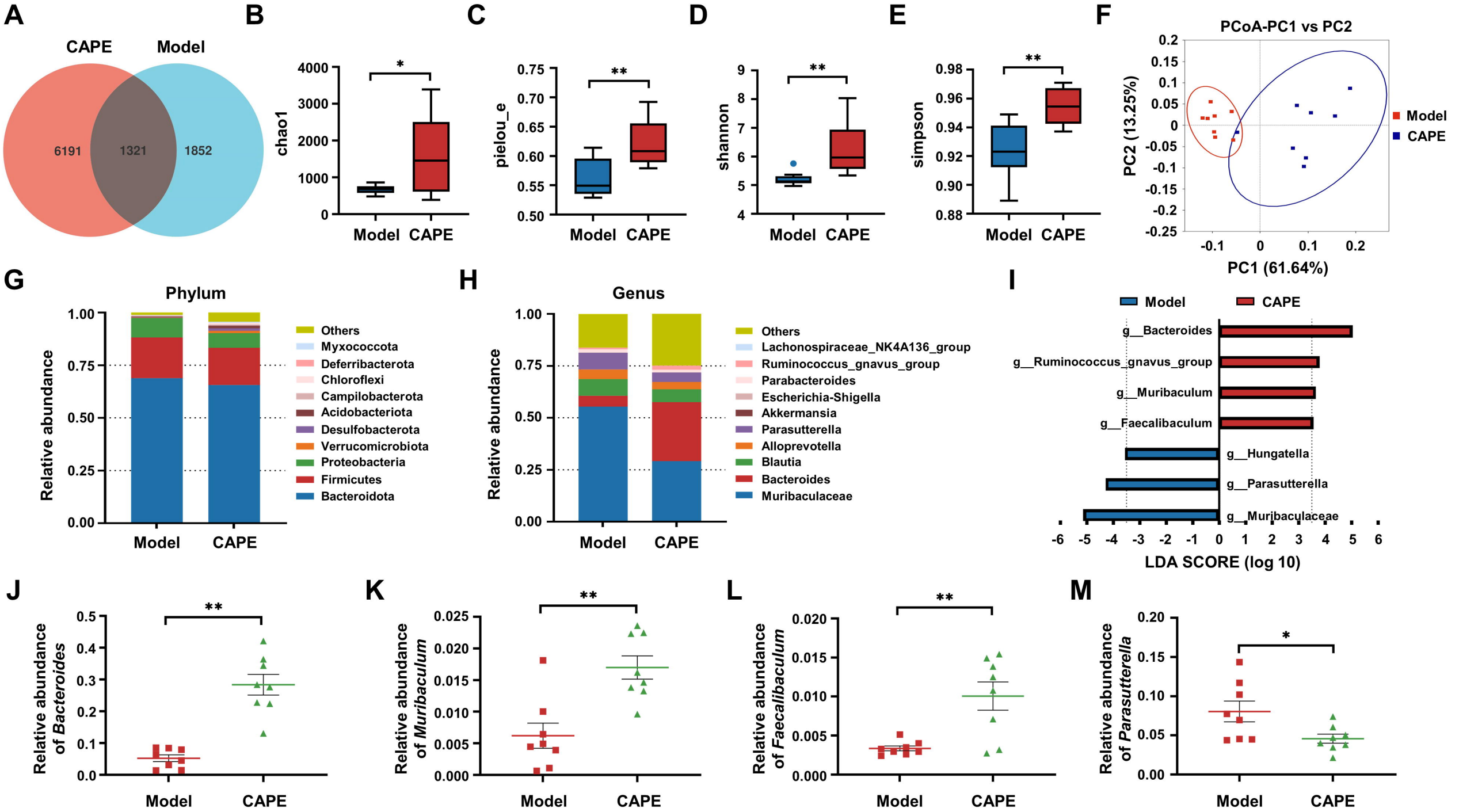
A
CAPE
Model
6191
1321
1852
B
chao1
Model
CAPE
C
pielou_e
D
shannon
E
simpson
F
PCoA-PC1 vs PC2
PC2 (13.25%)
PC1 (61.64%)
Model
CAPE
G
Phylum
Relative abundance
Others
Myxococcota
Deferribacterota
Chloroflexi
Campilobacterota
Acidobacteriota
Desulfobacterota
Verrucomicrobiota
Proteobacteria
Firmicutes
Bacteroidota
H
Genus
Relative abundance
Others
Lachonospiraceae_NK4A136_group
Ruminococcus_gnavus_group
Parabacteroides
Escherichia-Shigella
Akkermansia
Parasutterella
Alloprevotella
Blautia
Bacteroides
Muribaculaceae
I
Model
CAPE
g__Bacteroides
g__Ruminococcus_gnavus_group
g__Muribaculum
g__Faecalibaculum
g__Hungatella
g__Parasutterella
g__Muribaculaceae
LDA SCORE (log 10)
J
Relative abundance of Bacteroides
K
Relative abundance of Muribaculum
L
Relative abundance of Faecalibaculum
M
Relative abundance of Parasutterella

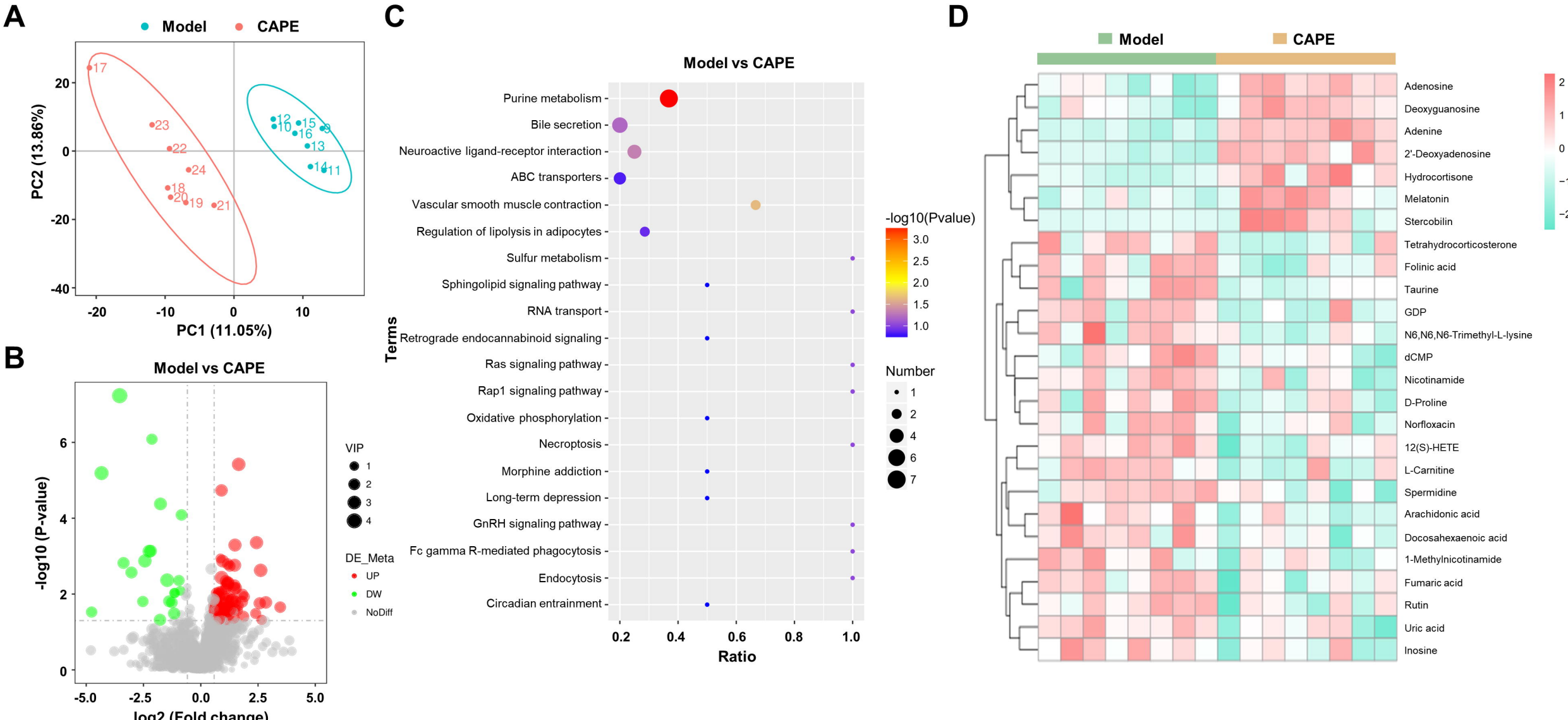
A
Model
CAPE
PC2 (13.86%)
PC1 (11.05%)
B
Model vs CAPE
-log10 (P-value)
log2 (Fold change)
VIP
DE_Meta
UP
DW
NoDiff
C
Model vs CAPE
Purine metabolism
Bile secretion
Neuroactive ligand-receptor interaction
ABC transporters
Vascular smooth muscle contraction
Regulation of lipolysis in adipocytes
Sulfur metabolism
Sphingolipid signaling pathway
RNA transport
Retrograde endocannabinoid signaling
Ras signaling pathway
Rap1 signaling pathway
Oxidative phosphorylation
Necroptosis
Morphine addiction
Long-term depression
GnRH signaling pathway
Fc gamma R-mediated phagocytosis
Endocytosis
Circadian entrainment
Terms
Ratio
-log10(Pvalue)
Number
D
Model
CAPE
Adenosine
Deoxyguanosine
Adenine
2'-Deoxyadenosine
Hydrocortisone
Melatonin
Stercobilin
Tetrahydrocorticosterone
Folinic acid
Taurine
GDP
N6,N6,N6-Trimethyl-L-lysine
dCMP
Nicotinamide
D-Proline
Norfloxacin
12(S)-HETE
L-Carnitine
Spermidine
Arachidonic acid
Docosahexaenoic acid
1-Methylnicotinamide
Fumaric acid
Rutin
Uric acid
Inosine

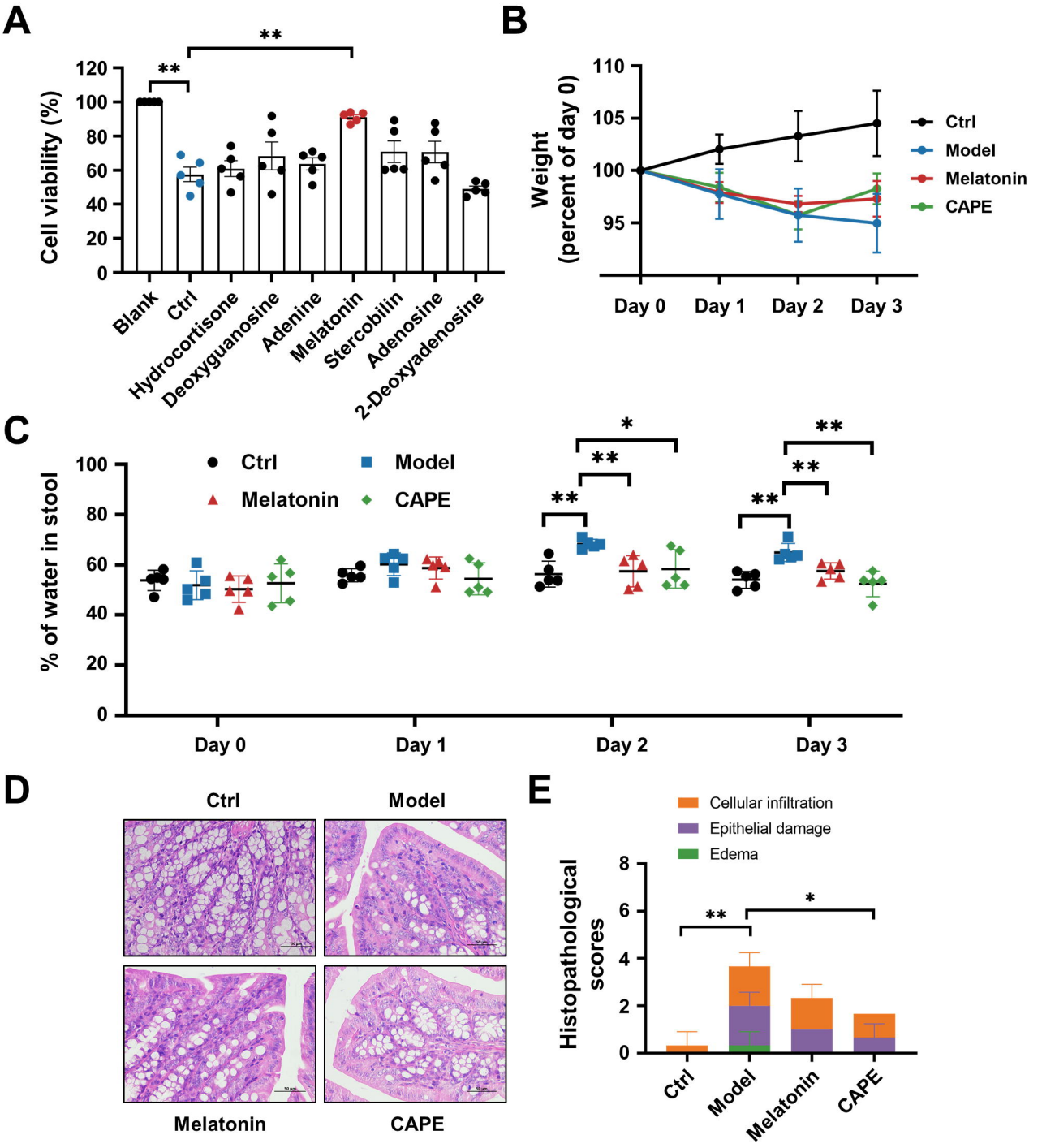
A
Cell viability (%)
120
100
80
60
40
20
0
**
**
Blank
Ctrl
Hydrocortisone
Deoxyguanosine
Adenine
Melatonin
Stercobilin
Adenosine
2-Deoxyadenosine
B
Weight (percent of day 0)
110
105
100
95
Day 0
Day 1
Day 2
Day 3
Ctrl
Model
Melatonin
CAPE
C
% of water in stool
100
80
60
40
20
0
Ctrl
Model
Melatonin
CAPE
Day 0
Day 1
Day 2
Day 3
D
Ctrl
Model
Melatonin
CAPE
E
Cellular infiltration
Epithelial damage
Edema
Histopathological scores
8
6
4
2
0
**
*
Ctrl
Model
Melatonin
CAPE

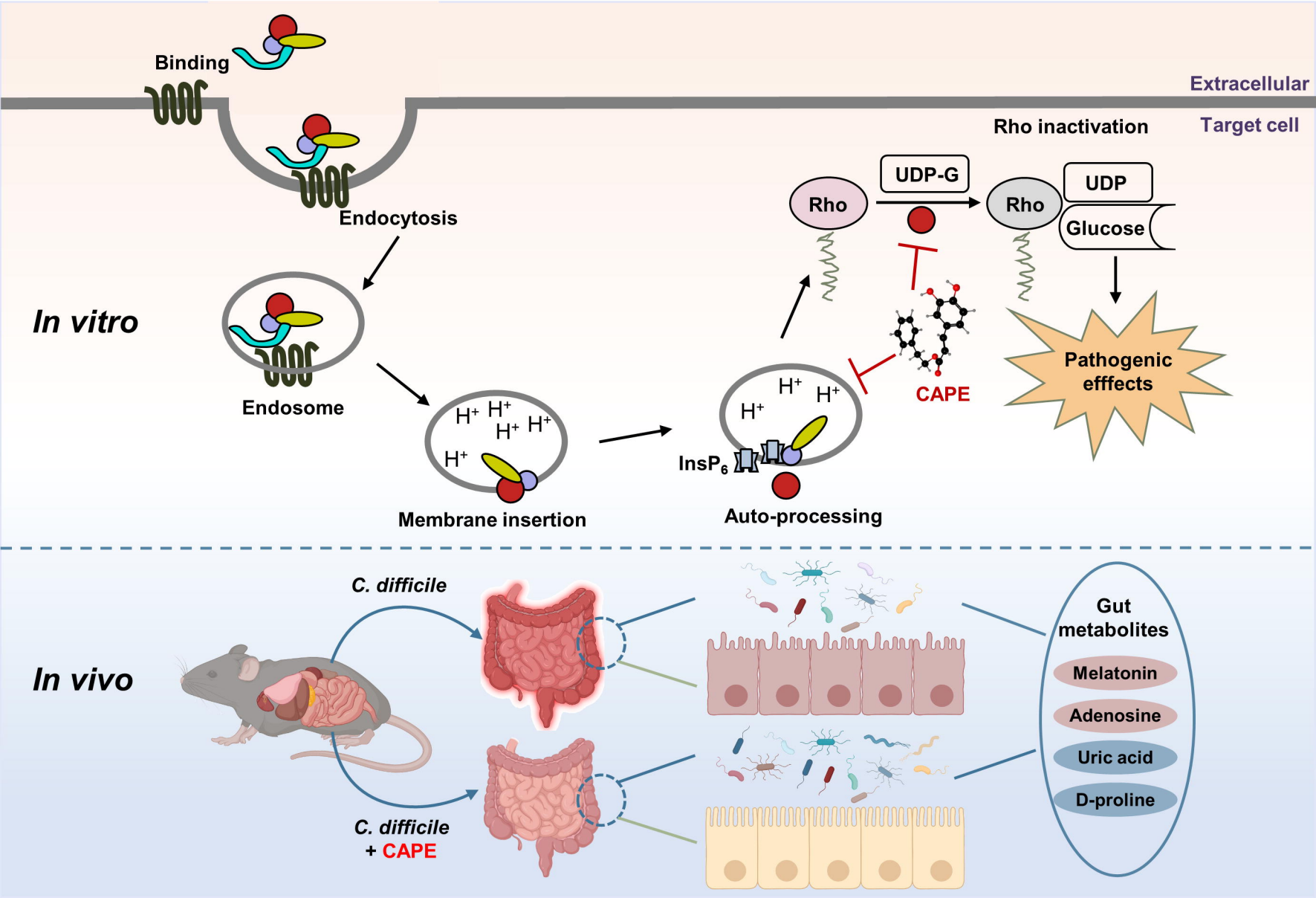
Binding
Extracellular
Target cell
Endocytosis
Rho inactivation
UDP-G
Rho
Rho
UDP
Glucose
In vitro
Endosome
H+
Membrane insertion
InsP6
Auto-processing
CAPE
Pathogenic
efffects
In vivo
C. difficile
C. difficile
+ CAPE
Gut
metabolites
Melatonin
Adenosine
Uric acid
D-proline

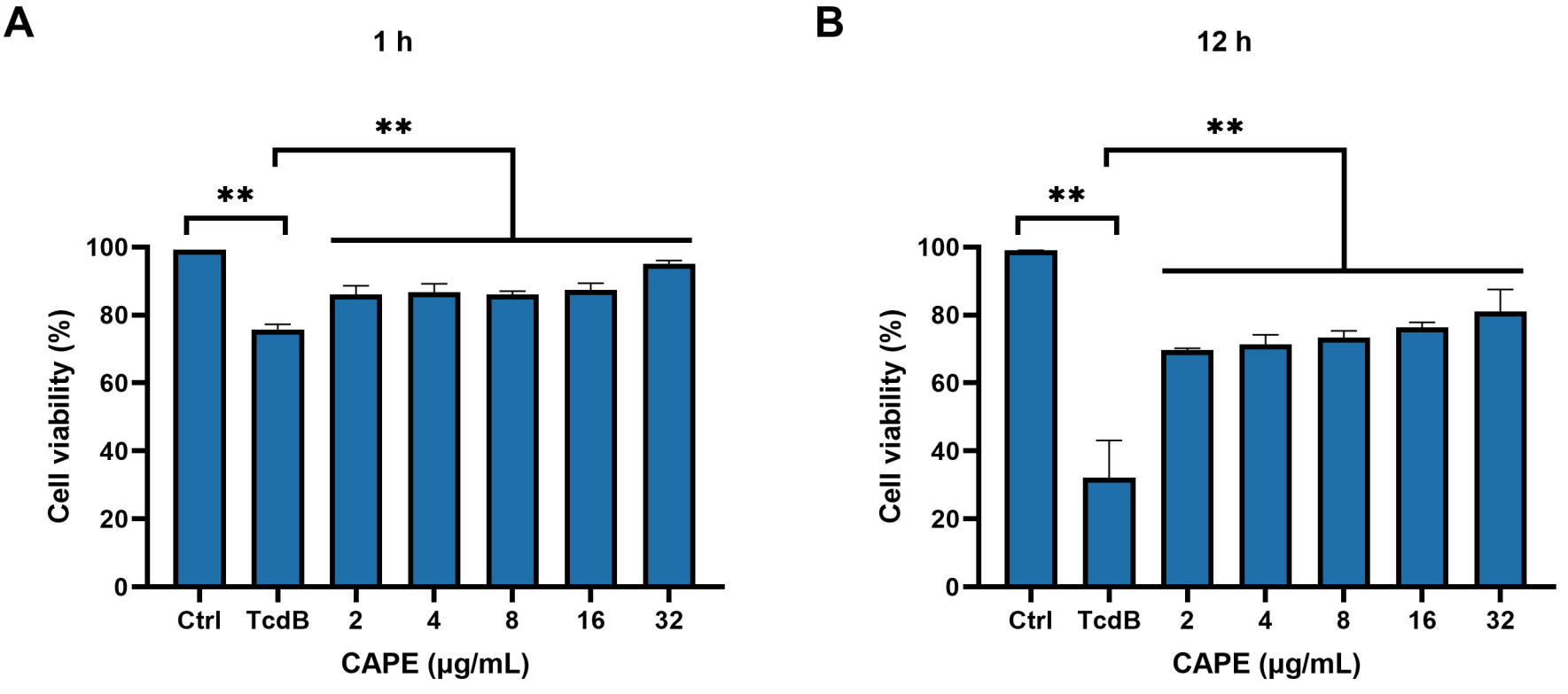
A
1 h
**
**
100
80
60
40
20
0
Cell viability (%)
Ctrl
TcdB
2
4
8
16
32
CAPE (μg/mL)
B
12 h
**
**
100
80
60
40
20
0
Cell viability (%)
Ctrl
TcdB
2
4
8
16
32
CAPE (μg/mL)

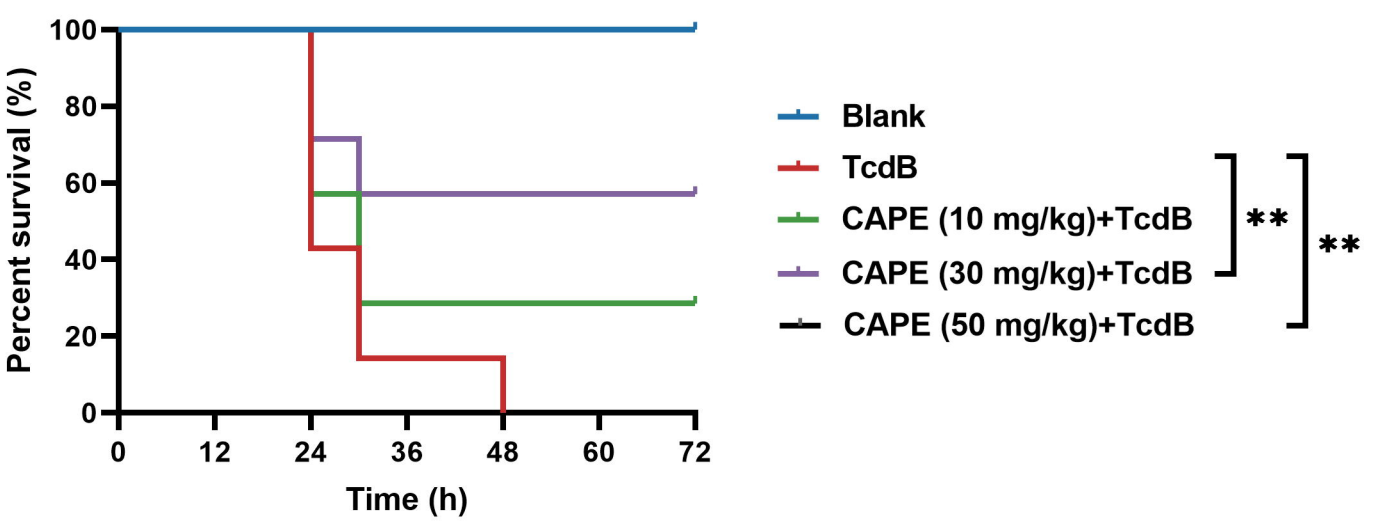
Percent survival (%)
100
80
60
40
20
0
0
12
24
36
48
60
72
Time (h)
Blank
TcdB
CAPE (10 mg/kg)+TcdB
CAPE (30 mg/kg)+TcdB
CAPE (50 mg/kg)+TcdB
**
**

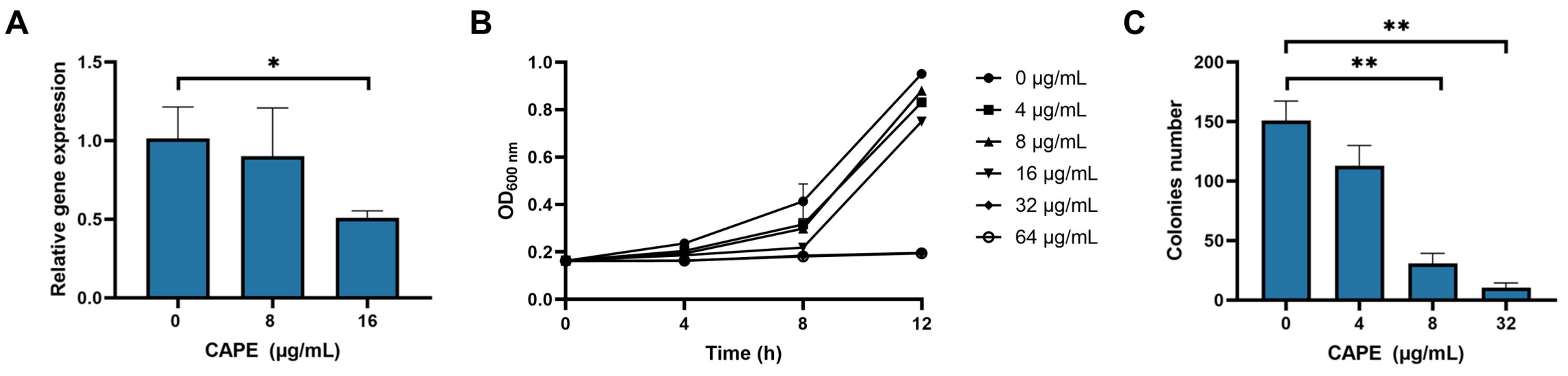
A
Relative gene expression
1.5
1.0
0.5
0.0
*
0
8
16
CAPE (μg/mL)
B
OD600 nm
1.0
0.8
0.6
0.4
0.2
0.0
0
4
8
12
Time (h)
0 μg/mL
4 μg/mL
8 μg/mL
16 μg/mL
32 μg/mL
64 μg/mL
C
Colonies number
200
150
100
50
0
**
**
0
4
8
32
CAPE (μg/mL)

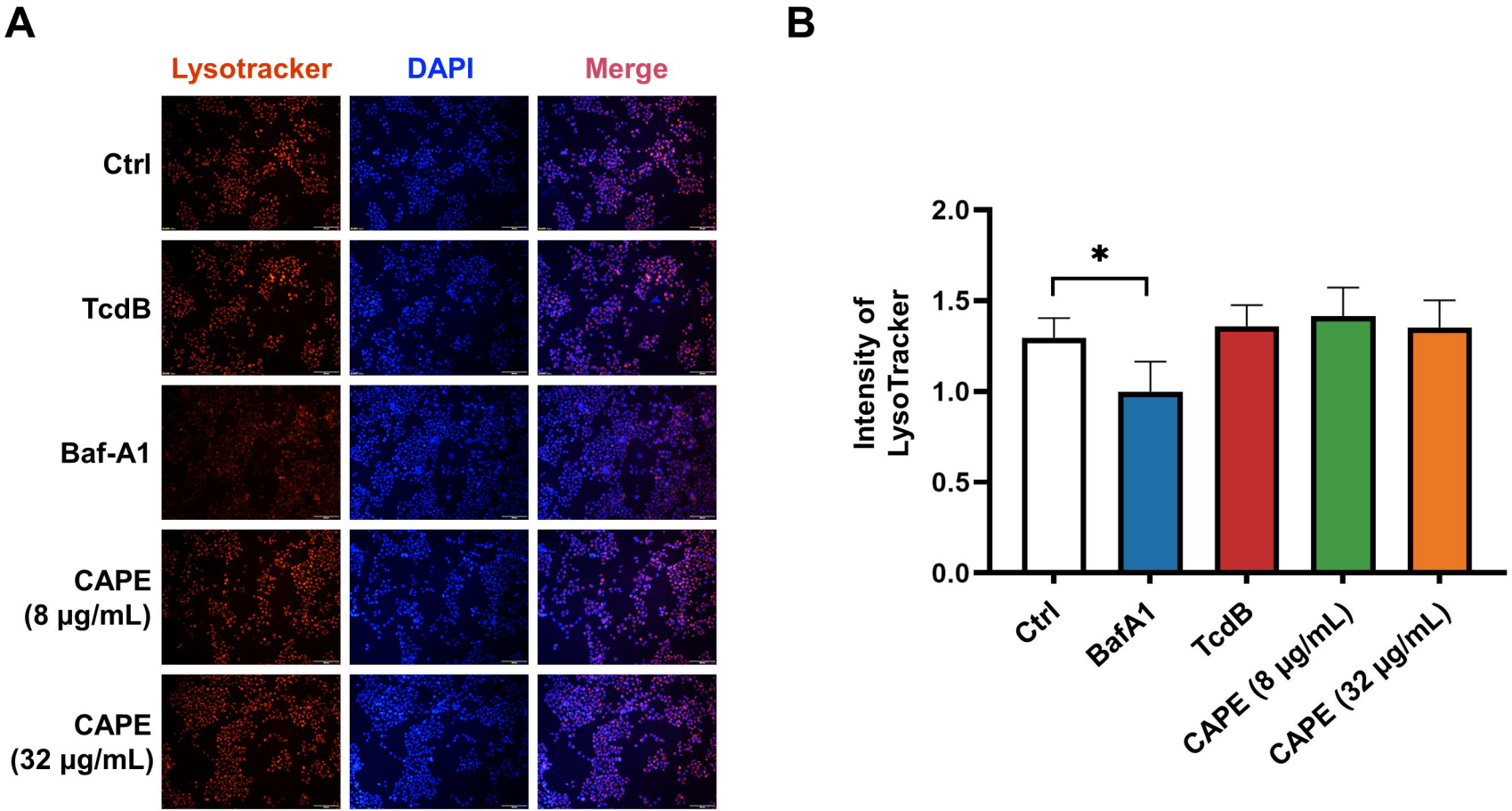
A
Lysotracker
DAPI
Merge
Ctrl
TcdB
Baf-A1
CAPE
(8 μg/mL)
CAPE
(32 μg/mL)
B
Intensity of
LysoTracker
2.0
1.5
1.0
0.5
0.0
*
Ctrl
BafA1
TcdB
CAPE (8 μg/mL)
CAPE (32 μg/mL)

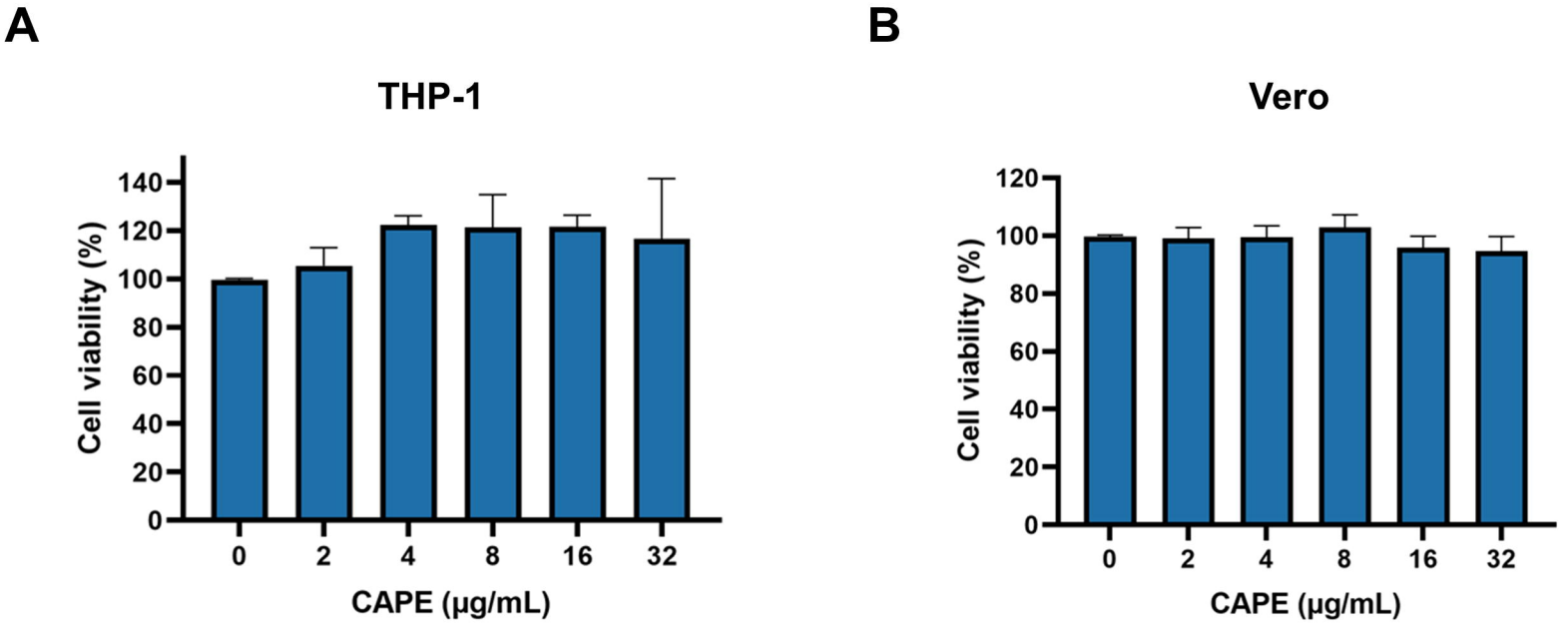
A
THP-1
Cell viability (%)
140
120
100
80
60
40
20
0
0
2
4
8
16
32
CAPE (µg/mL)
B
Vero
Cell viability (%)
120
100
80
60
40
20
0
0
2
4
8
16
32
CAPE (µg/mL)

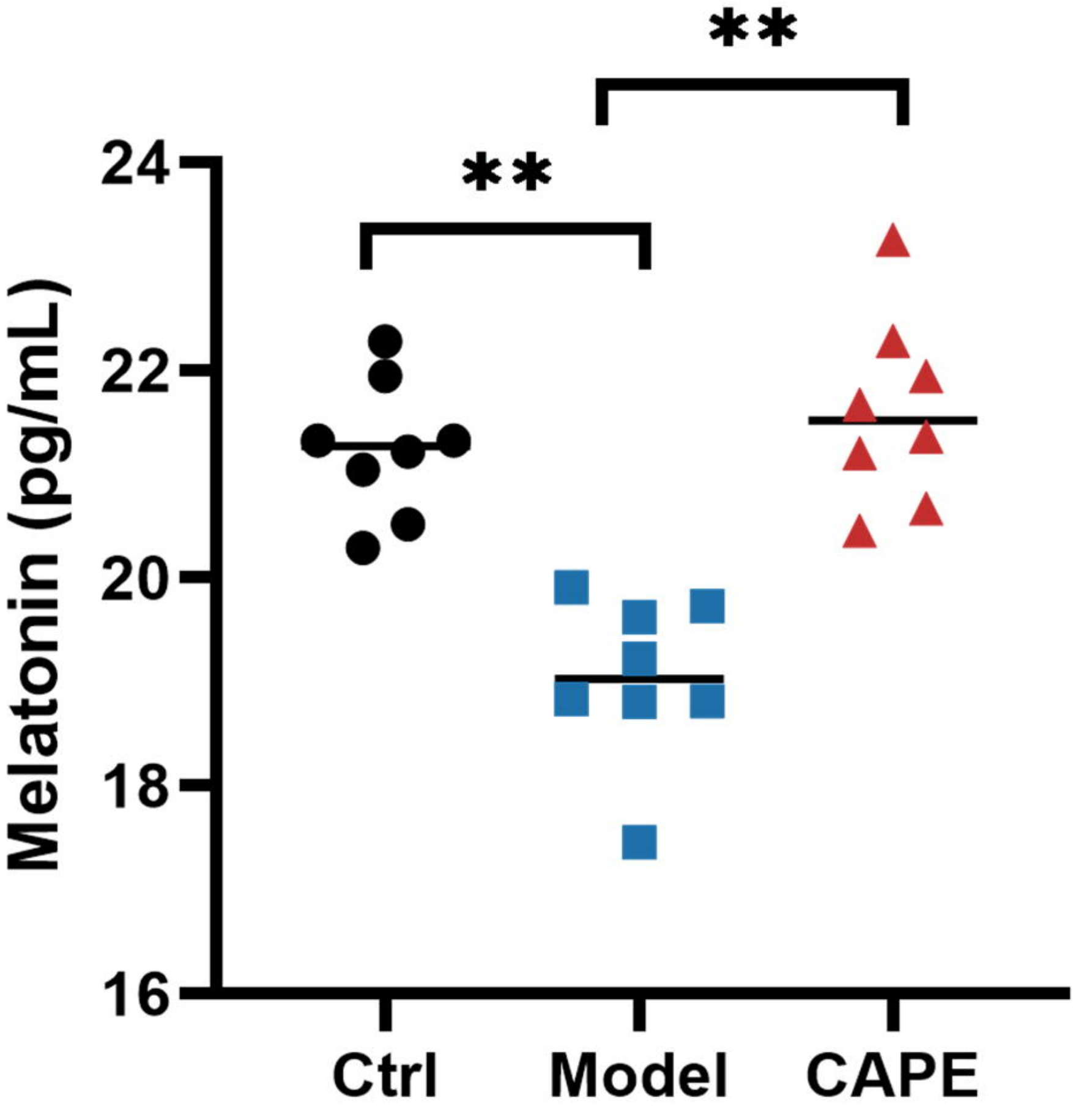
**
**
24
22
20
18
16
Melatonin (pg/mL)
Ctrl
Model
CAPE

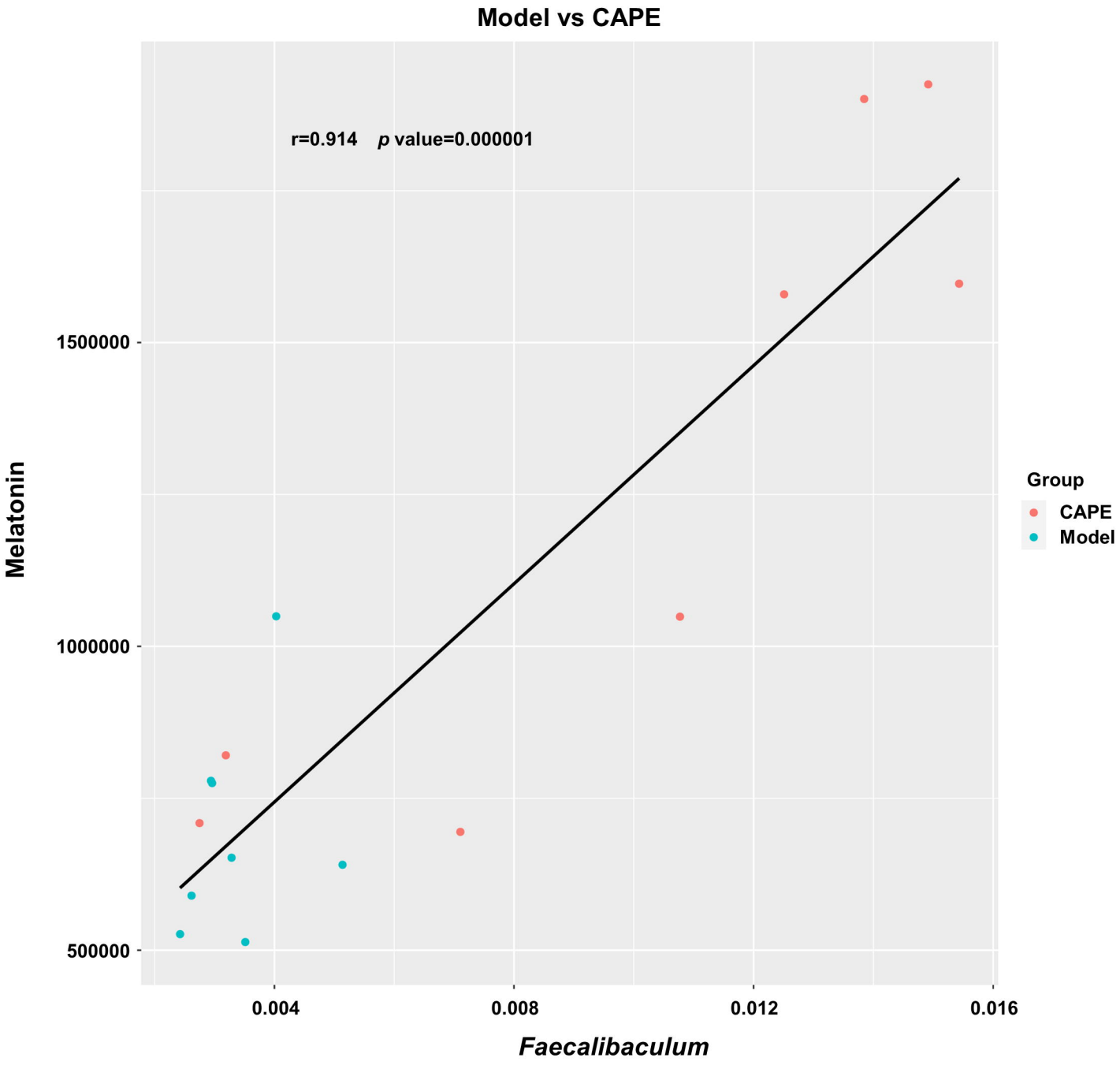
Model vs CAPE
r=0.914 p value=0.000001
Melatonin
1500000
1000000
500000
0.004
0.008
0.012
0.016
Faecalibaculum
Group
CAPE
Model

Table S1. IC_{50} of the caffeic acid and its derivate on TcdB-mediated cell-rounding.

Compound	Structure	IC_{50} (μg/mL)
Caffeic acid	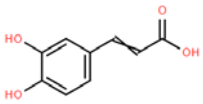	527.5
Ethyl caffeate	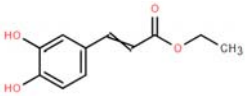	5.9
CAPE	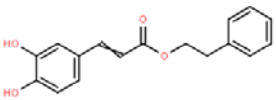	3.0
Echinacoside	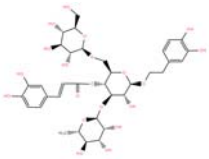	5.1
Rosmarinic acid	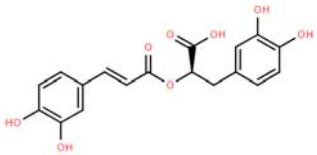	198.1
Salvianolic acid	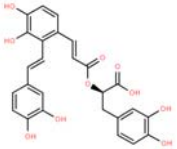	3.4
Verbascoside	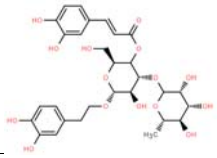	5.4

Table S2. Primers used in this study.

Primers	Sequences	Notes
YG101	ctgGGATCCATGAGTTTAGTTAATAG	*gtd* BamHI-F
YG102	ctgGTCGACCTAAAGAGAACCTTCAA	*gtd* SalI-R
YG103	CAGAAGCAGCAGCTGCATTCCACCTTTCTACC AACTCTTGTTC	gtd_{L265A} -F
YG104	GAACAAGAGTTGGTAGAAAGGTGGAATGCAG CTGCTGCTTCTG	gtd_{L265A} -R
YG105	GTATTCCTGGTAACATATCAACAGCTAAATACAT ACCACCAATTTCT	gtd_{D286A} -F
YG106	AGAAATTGGTGGTATGTATTTAGCTGTTGATAT GTTACCAGGAATAC	gtd_{D286A} -R
YG107	CAGGGCCACTTAAGTTAATAGCAGTTTTAACAT CTGGGAAGAA	gtd_{T465A}-F
YG108	TTCTTCCCAGATGTTAAAACTGCTATTAACTTA AGTGGCCCTG	gtd_{T465A}-R
YG109	TGCTTCAGGGCCACTTAAGTTAGCAGTAGTTT TAACATCTGGGAAG	gtd_{I466A}-F
YG110	CTTCCCAGATGTTAAAACTACTGCTAACTTAAG TGGCCCTGAAGCA	gtd_{I466A}-R
YG111	CTTGCATCGTCAAATGACCATGCGCTAGCCAT TTCTTGTTCAGT	gtd_{L519} -F
YG112	ACTGAACAAGAAATGGCTAGCGCATGGTCATT TGACGATGCAAG	gtd_{L519A} -R
YG113	CTCTTGCATCGTCAAATGACGCTAAGCTAGCC ATTTCTTGTTC	gtd_{W520A} -F
YG114	GAACAAGAAATGGCTAGCTTAGCGTCATTTGA CGATGCAAGAG	gtd_{W520A}-R

Table S3. Sequence of primers used for Reverse transcriptase PCR (RT-PCR) analysis.

Gene	Primer	Sequence (5'-3')
tcdB	Forward	TAGCAAGAAGTTCAGAGAGAGGAT
	Reverse	CTTGTATTTCACCATCTCCAGGA
16S	Forward	GCGTAGGCGGTCTTTCAAG
	Reverse	TCGCAACTGGTGTTCCTCC